

The masses, and the mass discrepancy of O-type stars

Carsten Weidner¹ and Jorick S. Vink²

¹ Scottish Universities Physics Alliance (SUPA), School of Physics and Astronomy, University of St Andrews, North Haugh, St Andrews, Fife KY16 9SS, UK e-mail: cw60@st-andrews.ac.uk

² Armagh Observatory, College Hill, Armagh BT61 9DG, UK e-mail: js.vink@arm.ac.uk

Received 2010 / Accepted 2010

ABSTRACT

Context. The “mass discrepancy” in massive O stars represents a long-standing problem in stellar astrophysics with far-reaching implications for the chemical and dynamical feedback in galaxies.

Aims. Our goal is to investigate this mass discrepancy by comparing state-of-the-art model masses with model-independent masses determined from eclipsing binaries.

Methods. Using stellar evolution models and a recent calibration of stellar parameters for O-star spectral sub-classes, we present a convenient way to convert observed solar metallicity O star spectral types into model masses, which we subsequently compare to our dynamical mass compilation. We also derive similar conversions for Large and Small Magellanic Cloud metallicities.

Results. We obtain a good agreement between model and dynamical masses, suggesting the long-standing problem of a systematic mass discrepancy problem may have been solved. We also provide error ranges for the model masses, as well as minimal and maximal age estimates for when the model stars are in a given spectral type box.

Key words. binaries: close – binaries: eclipsing – stars: early-type – stars: evolution – stars: formation – stars: fundamental parameters

1. Introduction

The most basic parameter of a star is its mass. Knowledge of this most fundamental parameter is of utmost importance for basically all of astrophysics. For massive O stars, reliable mass determinations have turned out to be particularly challenging. For over two decades there has been a “mass discrepancy” where O-star masses derived from evolutionary models (M_{evol}) were found to be systematically higher than those derived from stellar atmosphere analyses (M_{spec}) by up to a factor ~ 2 (Groenewegen & Lamers 1989; Herrero et al. 1992). Even two recent studies still report a significant mass discrepancy for non-enriched O-type stars in the Large Magellanic Cloud (LMC, Mokiem et al. 2007) and the Milky Way (MW, Hohle et al. 2010).

Over the last few decades, four alternative methods to determine O star masses have been developed:

- evolutionary masses (M_{evol})
- spectroscopic masses (M_{spec})
- wind masses (M_{wind})
- dynamical masses (M_{dyn}).

In the first method, one places the luminosity (or absolute magnitude) and effective temperature (or colour) in a Hertzsprung-Russell diagram (HRD) and compares the positions of the stars with theoretical stellar evolution models.

The second way comprises the use of stellar spectroscopy: via the Stark broadening in spectral lines, one can derive log g and subsequently the mass M_{spec} . For O stars, this method is highly complex, because stellar winds have a severe influence on the underlying model atmospheric structure (e.g. Gabler et al. 1989; Hillier 1991).

In the meantime, a third method to determine O star wind masses M_{wind} had been put forward (Groenewegen & Lamers

1989; Kudritzki et al. 1992). This method employs the radiation-driven theory (e.g. Castor et al. 1975), which relates the terminal wind velocity to the stellar escape velocity. Kudritzki et al. (1992) and Herrero et al. (1992) found good agreement between their spectroscopic and wind masses, and suggested that the evolutionary masses were systematically too large. Although there was indeed no particular reason to expect that evolutionary masses should be correct – given the large number of uncertainties in the underlying physical input (e.g. mass loss, overshooting, rotation, and magnetic effects) – the evolutionary calculations seemed to reproduce the observed O-star properties rather well (Hilditch et al. 1996). Subsequent work by Burkholder et al. (1997), who tried to derive masses from binary dynamics (M_{dyn}), suggested that the evolutionary masses were at least of the right order of magnitude, thereby challenging the spectroscopic masses, which were significantly lower at the time.

The best argument to trust the spectroscopic masses was their independent agreement with wind masses based on radiation-driven wind theory. This was not always the case as in the 1990s, there was also a systematic discrepancy between mass-loss rates predicted by wind theory and observations (Lamers & Leitherer 1993; Puls et al. 1996). This situation changed when Vink et al. (2000) presented new wind models including multiple-scattering. These models no longer show the systematic discrepancy with empirical rates¹. Although the good agreement reached between these new mass-loss predictions and the empirical rates – using the evolutionary rather than the spectroscopic masses – could have been coincidental, the additional

¹ Although it is currently debated whether the absolute values of these mass-loss rates are of the right order of magnitude. Some recent studies have called for a fundamental reduction in O-star mass-loss rates as a result of wind clumping (Bouret et al. 2005; Fullerton et al. 2006).

compatibility between evolutionary and dynamical masses, resulting in an agreement between *three* methods, led to the suspicion that it was most likely the spectroscopic masses that were the main culprit for the mass discrepancy.

Lanz et al. (1996) had already suggested that the neglect of line-blanketing could cause M_{spec} to be underestimated, and subsequent improvements resulted in a new calibration of Galactic O-star parameters by Martins et al. (2005, hereafter MSH05). These state-of-the-art non-local thermodynamic equilibrium (NLTE) models include both mass loss and line-blanketing. In the meantime, the effects of stellar rotation were included in the Geneva evolutionary models (Meynet & Maeder 2003), and below we will indeed confirm that the evolutionary masses now agree with the spectroscopic ones. This should be considered a major triumph for the formidable task of including full Fe line-blanketing in the atmospheric models (e.g. Hillier et al. 2003).

Nevertheless, given that both the Geneva evolutionary masses and the MSH05 calibration include the same Vink et al. (2000) mass-loss rates, even an agreement with the wind masses could be a coincidence involving complex model interdependences, and it is by no means certain they should be correct. It thus remains crucial to check our model masses against model-independent ones.

The only known model-independent masses so far are the dynamically derived ones: M_{dyn} . This method is only applicable to binary stars. Usually, careful determination of the orbital parameters of a system allows one to obtain the mass ratio of the two stars, as the orbit inclination relative to Earth is generally unknown. Only for eclipsing binaries, the inclination is well-enough constrained to be able to measure absolute stellar masses. Unfortunately, stars eclipsing each other are very rare, and the search for these systems comprises an important endeavor to calibrate and verify evolutionary models. In this paper we provide a compilation of dynamical masses derived from eclipsing binaries. Only very few eclipsing binaries are known that composed of at least one massive star². All of these are challenging to study because they are distant and, as most or probably all massive stars are born in star clusters (Adams & Myers 2001; Lada & Lada 2003; Allen et al. 2007), in very crowded regions of the sky. Nonetheless, a growing sample of eclipsing O stars is known, and we intend to use these to calibrate a relation between the spectral type of an O star and its present-day mass. Such a relation allows us also to calibrate the masses of O stars that are not part of an eclipsing binary system, i.e. the vast majority!

In Sect. 2 the spectral classification of O stars is discussed, while in Sect. 3 the mass determinations from eclipsing binaries and spectroscopic masses are presented. The results of this study follows in Sect. 4, and a summary is provided in Sect. 5. The stellar evolution models used and our interpolation scheme for additional intermediate model masses is described in appendix A. Furthermore, a large table is provided in the appendix B, which shows the spectral type evolution of the different stellar models used (on-line only).

2. Spectral classification of massive stars

Traditionally, O star spectral types are divided into sub-types from O3 to O9, with 0.5 steps (but without the sub-types O3.5 and O4.5). These are observationally defined by the relative

strength of the HeI to HeII lines (Conti & Alschuler 1971). Walborn et al. (2002) additionally defined the early O2, O2.5 and O3.5 subtypes, but because the O2 sub-type classification involves the nitrogen (N) sequence rather than the He sequence, these additional sub-types are not (yet) universally accepted. For instance, MSH05 do not use them. For numerical simplicity, we employ the range of sub-types O2 to O9.5, divided into bins of 0.5 width, and with luminosity classes: V (main-sequence), III (giant), and I (supergiant).

These sub-type-luminosity-classes (from now on spectral type boxes) are defined by six vertices each, the four corner points and the mean values between the central points of each box. Each vertice is described by a luminosity and a T_{eff} . *Panel MW* of Fig. 1 shows these boxes for the solar metallicity grid. The central points of the boxes (marked with *crosses*) are the new O star spectral type calibrations by MSH05. Table 1 shows the values of the vertices for the solar metallicity spectral boxes. As the subtypes O3.5 and O4.5 are not provided by MSH05, the corresponding values (shown as *black dots* in *Panel A* of Fig. 1) are derived by interpolation between O3 and O4, and O4 and O5, respectively. For the O2 and O2.5 subtypes, which are not used by MSH05, their results are extrapolated to these classes (*open circles* in *Panel A* of Fig. 1). The following fits to their theoretical T_{eff} calibration are used to define the T_{eff} values for O2 and O2.5 for the three luminosity classes:

$$\begin{aligned} \text{Class I : } T_{\text{eff}} &= 48598 - (ST * 2016) \\ \text{Class III : } T_{\text{eff}} &= 49045 - (ST * 2034) \\ \text{Class V : } T_{\text{eff}} &= 50941 - (ST * 1978), \end{aligned} \quad (1)$$

where ST is the spectral subtype. With these T_{eff} values and MSH05 Eqs. (3), (4) and (5), the corresponding luminosities are calculated. The upper limit for the supergiants is set by the empirical hot edge of the Luminous Blue Variables (LBV) from Smith et al. (2004) $\log_{10}(L_{\text{LBVmin}}) = 2.2056 \cdot \log_{10}(T_{\text{eff}}) - 3.7737$. If a star is above this line it is regarded to be an LBV. The lower limit is somewhat arbitrarily set as a parallel line to the luminosity class V, shifted towards higher temperatures. The border between the O9.5 and B0 subclasses is set by the B0 definitions from Zorec et al. (2009) for the T_{eff} and the luminosities from Searle et al. (2008). Whenever a star is earlier than O2, it is designated O2.0 If* in the Tables 4 to 7 and 9.

Naturally, such a scheme is not to be expected to be in full compliance with how the spectral indices for O stars change with T_{eff} . To compensate for this, a general error of 1000K is assumed for all T_{eff} values used.

About one third of the stars with dynamical mass estimates (Table 2) are located in the LMC. This dwarf galaxy has a considerably lower metallicity than solar ($z_{\text{LMC}} \approx 0.008$, van den Bergh 2000) and therefore solar metallicity spectral definitions and evolutionary models might not represent these stars well. Especially the T_{eff} scale of LMC metallicity stars is well above solar metallicity ones (Evans 2009). As a comprehensive study of O type spectral classes like MSH05 does not exist for LMC metallicity stars, the sample of LMC O and early B-type stars of Mokiem et al. (2007) is used to fit the following relations between T_{eff} and $\log_{10}(L)$ for LMC metallicity O stars.

$$\begin{aligned} \text{Class I (LMC) : } T_{\text{eff}} &= 50597 - (ST * 2197) \\ \text{Class III (LMC) : } T_{\text{eff}} &= 53713 - (ST * 2432) \\ \text{Class V (LMC) : } T_{\text{eff}} &= 56143 - (ST * 2437). \end{aligned} \quad (2)$$

$$\text{Class I (LMC) : } \log_{10}(L) = 6.269 - (ST * 0.08698)$$

$$\text{Class III (LMC)} : \log_{10}(L) = 6.170 - (ST * 0.11850) \quad (3)$$

$$\text{Class V (LMC)} : \log_{10}(L) = 6.073 - (ST * 0.12877).$$

The resulting spectral type grid is shown in Table 1 and as *Panel LMC* of Fig. 1.

While there are no eclipsing binaries in Table 2 with SMC metallicities ($z_{\text{SMC}} \approx 0.004$, van den Bergh 2000), a recent T_{eff} calibration for O stars in the SMC does exist (Heap et al. 2006). Their data are used to derive the following T_{eff} and luminosity relations in dependence of the spectral subtype.

$$\text{Class I (SMC)} : T_{\text{eff}} = 48000 - (ST * 1857)$$

$$\text{Class III (SMC)} : T_{\text{eff}} = 47456 - (ST * 1715) \quad (4)$$

$$\text{Class V (SMC)} : T_{\text{eff}} = 51660 - (ST * 2092),$$

$$\text{Class I (SMC)} : \log_{10}(L) = 6.258 - (ST * 0.09048)$$

$$\text{Class III (SMC)} : \log_{10}(L) = 6.216 - (ST * 0.10763) \quad (5)$$

$$\text{Class V (SMC)} : \log_{10}(L) = 5.750 - (ST * 0.08798).$$

Like in the other two cases the spectral type grid is included in Table 1 and it is shown in *Panel SMC* of Fig. 1. As is visible in Fig. 1 and Table 1, the SMC T_{eff} grid is shifted to lower temperatures compared to the LMC grid. The reason for this is non-trivial, and deserves a thorough analysis using SMC metallicity NLTE atmospheres, which is beyond the scope of this paper. Note that the Heap et al. (2006) sample only includes one star with a spectral type earlier than O4. This star is not included in the relations, but the relations are used from O2 to O9.5.

In order to assign a certain spectral subtype and luminosity class to a specific evolutionary point in time, stellar evolution models from Meynet & Maeder (2003) (see also appendix A) are followed throughout the $T_{\text{eff}}-L$ -diagram. This is visualized in Fig. 2, where the luminosity- and T_{eff} -evolution for six rotating as well as non-rotating stellar models from 20 to 120 M_{\odot} (Meynet & Maeder 2003) are plotted (rotating models as *dashed lines* and non-rotating ones as *dotted lines*). In this figure, only the part of the evolution before the Wolf-Rayet (WR) stage is depicted. Objects that are still assumed to be core hydrogen are classified as WNL stars (Hamann et al. 2006). However, we note that the WNL classification is only used in appendix B. The present-day mass of a model during its evolution through a spectral subclass is from now on referred to as evolutionary mass (M_{evol}).

Table 4 shows the new spectral type mass conversion, based on solar metallicity rotating evolutionary models from 10 to 120 M_{\odot} (Meynet & Maeder 2003). The rotating models have initial rotational velocities ($v_{\text{rot ini}}$) of 300 km/s, which results in v_{rot} during the Main-Sequence evolution of 180 to 240 km/s. These velocities are within the range observed for O stars (Mokiem et al. 2006). A table with non-rotating models is provided as Table 5. As the Meynet & Maeder (2003) models only provide a limited mass resolution, a special interpolation routine (described in detail in appendix A) is deployed in order to provide a mass resolution down to 1 M_{\odot} . For LMC metallicity Meynet & Maeder (2005) provide only four models (30, 40, 60 and 120 M_{\odot} , all rotating with 300 km/s), two additional models (15 and 20 M_{\odot}) are taken from the Padova group (Bertelli et al. 2009). The resulting spectral type mass conversion for LMC metallicity stars is shown in Table 6. For SMC metallicities, Meynet & Maeder (2003) only include three (all rotating) models (40, 60 and 120 M_{\odot}). Again, two models are added here (15

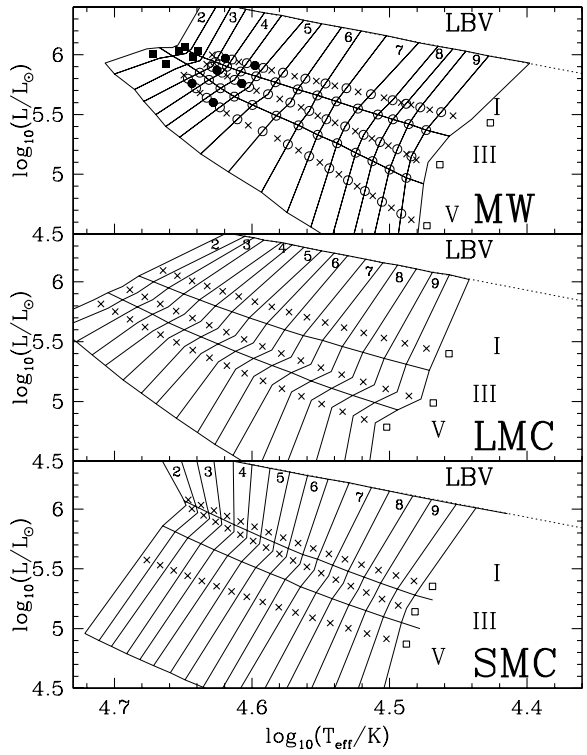


Fig. 1. Definitions of the solar metallicity O star spectral types in the luminosity-temperature diagram derived from MSH05 (*panel MW*), the LMC metallicity (*panel LMC*) and the SMC metallicity (*panel SMC*) derived in this work. *Panel MW* shows the original MSH05 data as crosses and the interpolated 3.5 and 4.5 subclasses as filled circles. Plotted as filled boxes are the extrapolated subtypes 2.5 and 2. The open circles connected by solid lines represent the interpolated grid that defines the L and T_{eff} values for each spectral subtype. The luminosity classes are indicated as Roman numerals (I - supergiants, III - giants and V - dwarfs), while the spectral subtypes are shown by Arabic numerals. The upper limit (dotted line) is given by the hot edge for luminous blue variables (LBV) given in Smith et al. (2004). All interpolations are derived by calculating mean values in linear space. *Panel LMC* shows the LMC metallicity grid derived from Mokiem et al. (2007) and *panel SMC* the one for SMC metallicity obtained from Heap et al. (2006).

and 20 M_{\odot}) from Bertelli et al. (2009) in order to derive a spectral type mass conversion (Table 7).

The masses shown in the Tables 4 to 7 are all weighted by the duration of the models in each spectral class. The errors are assigned by using the most- and least-massive model entering the spectral class. As mentioned before, each spectral class has an assumed error in T_{eff} of 1000 K. The minimal and maximal start and end ages give the range of possible ages for the stars in a spectral-class box. The advantage of using this method is the consistent application of observational constraints for the different evolutionary phases on one set of stellar evolution models. This allows one to place more constraints for the stars in a certain spectral class on the range of their initial and present-day masses.

A number of other mass estimates for spectral types exist in the literature, e.g. Vacca et al. (1996) and Hanson et al. (1997),

Table 1. Spectral type definitions.

Lum. class: Sp. type	I L_1	I L_2	I/III L_3	III L_4	III/V L_5	V L_6	V L_7	I $T_{\text{eff}1}$	I $T_{\text{eff}2}$	I/III $T_{\text{eff}3}$	III $T_{\text{eff}4}$	III/V $T_{\text{eff}5}$	V $T_{\text{eff}6}$	V $T_{\text{eff}7}$
Milky Way, $z = 0.02$														
2.0	6.45	6.08	6.07	6.06	6.06	6.05	5.93	43182.0	45070.5	45277.5	45484.5	46482.0	47479.5	50906.1
2.0/2.5	6.43	6.05	6.03	6.01	5.99	5.97	5.84	42128.0	44063.0	44265.2	44467.5	45479.0	46490.5	50119.0
2.5/3.0	6.41	6.02	5.98	5.95	5.92	5.88	5.71	41198.0	43055.0	43252.8	43450.5	44378.2	45306.0	48459.0
3.0/3.5	6.38	5.99	5.94	5.90	5.85	5.80	5.61	40221.0	42089.0	42333.5	42578.0	43447.5	44317.0	47698.0
3.5/4.0	6.35	5.96	5.90	5.85	5.79	5.72	5.50	38993.0	41164.5	41507.2	41850.0	42784.2	43718.5	46767.0
4.0/4.5	6.33	5.93	5.86	5.79	5.72	5.64	5.40	37883.0	40156.5	40574.0	40991.5	41970.5	42949.5	45987.0
4.5/5.0	6.29	5.89	5.82	5.73	5.65	5.56	5.31	36501.0	39065.5	39533.8	40002.0	41006.0	42010.0	44930.0
5.0/5.5	6.26	5.85	5.77	5.67	5.58	5.46	5.17	35426.0	37795.0	38275.0	38755.0	39778.0	40801.0	43384.0
5.5/6.0	6.23	5.80	5.71	5.60	5.49	5.36	5.02	34274.0	36408.5	36873.2	37338.0	38222.2	39106.5	41418.0
6.0/6.5	6.20	5.76	5.66	5.53	5.41	5.25	4.85	33161.0	35200.5	35684.5	36168.5	36828.5	37488.5	39197.0
6.5/7.0	6.16	5.72	5.61	5.46	5.33	5.15	4.68	31782.0	33990.0	34570.5	35151.0	35664.8	36178.5	37546.0
7.0/7.5	6.10	5.67	5.55	5.40	5.26	5.05	4.56	30118.0	32619.5	33341.0	34062.5	34518.8	34975.0	36067.0
7.5/8.0	6.07	5.62	5.50	5.33	5.18	4.95	4.45	29164.0	31461.0	32245.5	33030.0	33465.5	33901.0	34962.0
8.0/8.5	6.05	5.59	5.46	5.27	5.11	4.86	4.36	28443.0	30756.5	31443.8	32131.0	32541.8	32952.5	33796.0
8.5/9.0	6.03	5.56	5.42	5.21	5.04	4.77	4.26	27831.0	30036.5	30624.8	31213.0	31618.0	32023.0	32797.0
9.0/9.5	5.99	5.52	5.37	5.15	4.97	4.67	4.14	26781.0	28999.5	29741.8	30484.0	30745.0	31006.0	31476.0
9.5/B0.0	5.93	5.46	5.32	5.10	4.92	4.60	4.03	25003.0	27570.0	28610.2	29650.5	29872.2	30094.0	30458.0
LMC, $z = 0.008$														
2.0	6.41	6.12	6.05	5.96	5.91	5.85	5.68	41508.5	46752.5	48104.8	49457.0	50667.8	51878.5	55897.2
2.0/2.5	6.38	6.07	6.00	5.91	5.85	5.78	5.61	40283.8	45653.5	46947.2	48241.0	49450.2	50659.5	54943.8
2.5/3.0	6.37	6.03	5.95	5.85	5.79	5.72	5.50	39683.0	44555.0	45790.0	47025.0	48233.0	49441.0	53444.5
3.0/3.5	6.35	5.99	5.90	5.79	5.73	5.66	5.39	39022.4	43457.0	44633.0	45809.0	47016.0	48223.0	52034.5
3.5/4.0	6.33	5.94	5.85	5.73	5.66	5.59	5.30	37894.6	42358.5	43475.8	44593.0	45798.8	47004.5	50877.5
4.0/4.5	6.31	5.90	5.80	5.67	5.60	5.53	5.18	37213.6	41259.5	42318.2	43377.0	44581.2	45785.5	49402.0
4.5/5.0	6.29	5.86	5.75	5.61	5.54	5.46	5.07	36491.9	40161.0	41161.0	42161.0	43364.0	44567.0	47899.7
5.0/5.5	6.26	5.81	5.70	5.55	5.48	5.40	4.98	35433.6	39063.0	40004.0	40945.0	42147.0	43349.0	46752.2
5.5/6.0	6.24	5.77	5.65	5.49	5.42	5.33	4.86	34696.0	37964.5	38846.8	39729.0	40929.8	42130.5	45189.8
6.0/6.5	6.22	5.73	5.60	5.43	5.36	5.27	4.74	33924.5	36865.5	37689.2	38513.0	39712.2	40911.5	43611.8
6.5/7.0	6.19	5.68	5.55	5.37	5.30	5.21	4.64	32916.7	35767.0	36532.0	37297.0	38495.0	39693.0	42351.4
7.0/7.5	6.16	5.64	5.51	5.31	5.24	5.14	4.55	31972.0	34669.0	35375.0	36081.0	37278.0	38475.0	41106.1
7.5/8.0	6.14	5.60	5.46	5.25	5.17	5.08	4.42	31193.2	33570.5	34217.8	34865.0	36060.8	37256.5	39428.9
8.0/8.5	6.11	5.55	5.41	5.20	5.11	5.01	4.31	30225.8	32471.5	33060.2	33649.0	34843.2	36037.5	38048.1
8.5/9.0	6.08	5.51	5.36	5.14	5.05	4.95	4.19	29428.4	31373.0	31903.0	32433.0	33626.0	34819.0	36405.0
9.0/9.5	6.06	5.47	5.31	5.08	4.99	4.88	4.05	28610.5	30275.0	30746.0	31217.0	32409.0	33601.0	34681.6
9.5/B0.0	6.02	5.42	5.26	5.02	4.93	4.82	3.94	27671.5	29588.8	30001.0	31191.8	32382.5	33242.4	
SMC, $z = 0.004$														
2.0	6.53	6.10	6.07	6.03	5.86	5.60	4.96	46917.2	44750.0	44602.5	44455.0	46227.0	47999.0	52669.3
2.0/2.5	6.49	6.06	6.02	5.97	5.81	5.55	4.90	45049.5	43822.0	43709.5	43597.0	45275.0	46953.0	51428.8
2.5/3.0	6.46	6.01	5.97	5.92	5.76	5.51	4.85	43774.8	42893.5	42816.5	42739.5	44323.2	45907.0	50368.6
3.0/3.5	6.43	5.96	5.92	5.87	5.71	5.46	4.79	42452.5	41964.5	41923.5	41882.5	43371.8	44861.0	49111.0
3.5/4.0	6.40	5.92	5.87	5.81	5.66	5.42	4.74	41089.1	41036.0	41030.5	41025.0	42420.0	43815.0	48033.9
4.0/4.5	6.37	5.87	5.82	5.76	5.61	5.38	4.69	39810.7	40108.0	40137.5	40167.0	41468.0	42769.0	46941.5
4.5/5.0	6.34	5.83	5.77	5.71	5.56	5.33	4.63	38628.1	39179.5	39244.5	39309.5	40516.2	41723.0	45651.1
5.0/5.5	6.31	5.78	5.72	5.65	5.51	5.29	4.57	37368.2	38250.5	38351.5	38452.5	39564.8	40677.0	44529.7
5.5/6.0	6.28	5.74	5.67	5.60	5.46	5.24	4.51	36280.7	37322.0	37458.5	37595.0	38613.0	39631.0	43206.9
6.0/6.5	6.25	5.69	5.62	5.54	5.41	5.20	4.45	35050.1	36394.0	36565.5	36737.0	37661.0	38585.0	42054.0
6.5/7.0	6.22	5.65	5.58	5.49	5.35	5.16	4.41	33833.2	35465.5	35672.5	35879.5	36709.2	37539.0	41021.0
7.0/7.5	6.18	5.60	5.53	5.44	5.30	5.11	4.34	32587.5	34536.5	34779.5	35022.5	35757.8	36493.0	39633.7
7.5/8.0	6.15	5.56	5.48	5.38	5.25	5.07	4.28	31619.5	33608.0	33886.5	34165.0	34806.0	35447.0	38400.6
8.0/8.5	6.11	5.51	5.43	5.33	5.20	5.02	4.21	30408.0	32680.0	32993.5	33307.0	33854.0	34401.0	36963.8
8.5/9.0	6.08	5.47	5.38	5.27	5.15	4.98	4.15	29471.1	31751.5	32100.5	32449.5	32902.2	33355.0	35654.6
9.0/9.5	6.04	5.42	5.33	5.22	5.10	4.94	4.09	28277.4	30822.5	31207.5	31592.5	31950.8	32309.0	34292.1
9.5/B0.0	6.01	5.38	5.28	5.17	5.05	4.89	4.01	27363.6	29894.0	30314.5	30735.0	30999.0	31263.0	32750.0

but only the most recent one by MSH05 is used here. These models provide spectroscopic stellar masses that are derived from the stellar luminosity, L , and T_{eff} of NLTE stellar atmosphere models through

$$M = \frac{gR^2}{G},$$

where G equals Newton's gravitational constant, and g is the gravitational acceleration of the star at radius R :

$$R = \sqrt{\frac{L}{4\pi\sigma_R T_{\text{eff}}^4}}, \quad (7)$$

where σ_R is the Stefan-Boltzmann constant. Martins et al. (2005) provide two mass estimates, one for a theoretical T_{eff} cal-

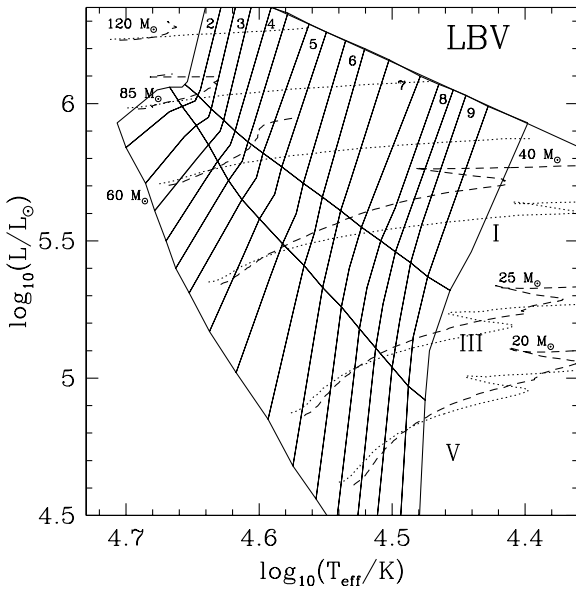


Fig. 2. Similar as panel A of Fig. 1, but only the spectral subtype boxes are shown as a grid of solid lines. The dashed lines are rotating and the dotted lines non-rotating solar metallicity stellar evolutionary tracks by Meynet & Maeder (2003) with initial masses as indicated in the figure. Only evolutionary phases before the Wolf-Rayet stage are plotted.

ibration ($m_{\text{MSH}1}$) and one for an observational T_{eff} calibration ($m_{\text{MSH}2}$).

Instead of using spectral type calibrations, a more direct way to derive spectroscopic masses is by carefully fitting model atmospheres to high-resolution spectra, where both g , and T_{eff} are determined simultaneously (see for example Repolust et al. 2004). Together with its absolute magnitude it is possible to arrive at a mass using Eqs. (6) and (7). A sample of spectroscopic masses derived with this method will also be compared with dynamical and model masses.

2.1. Limitations

Although the results presented here cover a large parameter space, they involve some caveats. First of all, both the employed Meynet & Maeder (2003) stellar evolution models, as well as the MSH05 stellar atmospheres, which define our spectral classes, only cover solar metallicity ($z = 0.02$). Metallicity is known to have a very strong influence on the evolution and atmospheres of (O) stars via their metallicity-dependent winds. The newly developed spectral type definitions for LMC and SMC metallicities are a first step to loosen these limitations, but are not as thoroughly based as the MSH05 work for solar metallicity.

Table 9 shows the spectral evolution of a series of massive stellar models of different metallicities ($z = 0.004, 0.008, 0.02$ and 0.04 , Meynet & Maeder 2003, 2005) using the spectral type definitions in Table 1. While these spectral type definitions are based on solar metallicity atmospheres or empirical T_{eff} calibrations (for $z = 0.008$ and $z = 0.004$), considerable differences in the evolution are noticeable.

Another relevant aspect for the evolution of massive stars concerns binary evolution. Because many (if not most) mas-

sive stars are part of a binary system, often with considerable secondary masses (Preibisch et al. 1999; Apai et al. 2007; Kobulnicky & Fryer 2007; Ritchie et al. 2009; Weidner et al. 2009; Sana et al. 2010), they could be capable of influencing each other's evolution in a profound manner. Because all observations presented in Table 2 involve eclipsing binaries, all the objects must form tight pairs with reasonably large stars, and therefore binary evolution is bound to be important, but it is a non-trivial matter to account for it.

As was mentioned in the introduction, an additional potential prime source for errors in the mass determination concerns the atmosphere and wind parameters, as well as the mass-loss prescription employed in the evolutionary models.

3. Dynamical masses of eclipsing binaries

In recent years, observational techniques allowed us to measure masses of very massive stars directly by observing the orbits of massive eclipsing binaries. In Table 2 the dynamical mass estimates for 33 very massive stars are listed. The majority of the stars (22) are from a compilation by Gies (2003), who provides three lists with massive binaries from the literature. His first list shows detached systems, the second one non-eclipsing binaries (with lower mass limits only) and the third systems, which are either dynamically evolved (semi-detached or contact systems) or contain giants or supergiants. All but two systems from the first list are included in Table 2 as are three systems from the third list, two of them are given as being before the interaction stage and the supergiant V729 Cyg. The systems with lower limits only and the ones which are dynamically evolved are not suitable for the current study and are therefore not included. The remaining eclipsing binaries except one are from literature published after the Gies (2003) list, but which contain the necessary data for this study. The exception is WR22 B, which is not covered in Gies (2003) because the primary is a Wolf-Rayet star.

The dynamical masses from Table 2 involve present-day masses instead of initial masses. This is accounted for by not only comparing the evolving parameters with the luminosity and T_{eff} grid, but by simultaneously keeping track of the initial mass. Therefore, in Table 4 the initial stellar mass for a spectral type is given as well as the possible minimal and maximal mass when the stars enter and leave the respective spectral type. Additionally, the minimal and maximal age is given when the models enter and leave a spectral type.

In addition to dynamical mass determinations, several spectroscopic masses exist for O-type stars. Table 3 shows a compilation of these spectroscopic masses taken from Repolust et al. (2004), besides the MSH05 masses and the evolutionary masses presented in this work.

4. Results and discussion

The Tables 4 and 5 show the determined initial masses as well as the mean, minimal, and maximal present-day masses according to the Meynet & Maeder (2003) rotating (300 km/s) and non-rotating stellar evolution models, and the MSH05 O star spectral type definition. Tables 6 and 7 show the same for LMC and SMC metallicities, respectively. The errors shown for the mass determination are the lowest mass and maximum mass models that pass through the spectral type. They also include an error margin of ± 1000 K for the MSH05 spectral type definitions. The differences in the supergiant mass errors from one subtype to the next have two main reasons. Spectral types later than O 6.5 I are

Table 2. Eclipsing O-star binaries with dynamical mass estimates.

Star	Sp Type	$m_{\text{dynamical}}$	m_{MSH1}	m_{MSH2}	m_{ini}	m_{evol}	m_{start}	m_{end}	Ref.
MW									
HD93205A	O3V	56.0± 4.0	58.3	58.0	67 -9/+9	65 -7/+7	67 -9/+6	64 -6/+8	(1)
FO15 A	O5.5V	30.0± 1.0	34.2	34.4	40 -7/+8	39 -6/+7	39 -6/+6	38 -5/+7	(2)
FO15 B	O9.5V	16.0± 1.0	16.5	15.6	18 -5/+4	18 -5/+4	18 -5/+4	18 -5/+4	(2)
Theta Orionis C1	O6Vpe	35.8± 7.2	31.7	31.0	35 -7/+6	34 -6/+5	34 -6/+5	33 -6/+6	(3)
V1036 Sco A	O6V	32.0± 4.0	31.7	31.0	35 -7/+6	34 -6/+5	34 -6/+5	33 -6/+6	(4)
V1036 Sco B	O7V	32.0± 4.0	26.5	25.3	28 -6/+8	27 -5/+7	27 -5/+6	27 -5/+7	(4)
LS1135 A	O6.5V	30.0± 1.0	29.0	28.0	31 -7/+6	30 -6/+6	30 -6/+5	30 -6/+6	(5)
V729 Cyg	O7Ianfp	47.0± 9.0	40.9	38.4	47 -9/+36	39 -5/+23	40 -6/+23	39 -5/+24	(4)
V1007 Sco A	O7.5III ^a	29.5± 0.4	29.1	27.4	33 -5/+6	31 -4/+4	31 -5/+4	31 -4/+5	(6)
V1007 Sco B	O7III ^a	30.1± 0.4	31.2	29.6	36 -5/+7	34 -4/+5	34 -4/+5	33 -4/+5	(6)
V3903 Sgr A	O7V	27.3± 6.0	26.5	25.3	28 -6/+8	27 -5/+7	27 -5/+6	27 -5/+7	(4)
V3903 Sgr B	O9V	19.0± 4.0	18.0	17.1	19 -5/+5	19 -5/+4	19 -5/+4	19 -5/+4	(4)
CPD -59 2603 A	O7V	22.7± 4.0 ^b	26.5	25.3	28 -6/+8	27 -5/+7	27 -5/+6	27 -5/+7	(4)
CPD -59 2603 B	O9.5V	14.5± 4.0 ^b	16.5	15.6	18 -5/+4	18 -5/+4	18 -5/+4	18 -5/+4	(4)
V1182 Aql A	O8Vnn	31.0± 0.6	21.9	20.8	23 -6/+6	22 -5/+6	22 -5/+6	22 -5/+6	(7)
EM Car A	O8V	22.9± 3.0	21.9	20.8	23 -6/+6	22 -5/+6	22 -5/+6	22 -5/+6	(4)
EM Car B	O8V	21.4± 3.0	21.9	20.8	23 -6/+6	22 -5/+6	22 -5/+6	22 -5/+6	(4)
CC Cas	O8.5III	18.3± 5.0	24.8	23.7	29 -5/+6	27 -4/+5	27 -4/+5	27 -4/+5	(4)
WR22 B	O9V	20.6± 1.7	18.0	17.1	19 -5/+5	19 -5/+4	19 -5/+4	19 -5/+4	(8)
V478 Cyg A	O9.5V	16.6± 9.0	16.5	15.6	18 -5/+4	18 -5/+4	18 -5/+4	18 -5/+4	(4)
V478 Cyg B	O9.5V	16.3± 9.0	16.5	15.6	18 -5/+4	18 -5/+4	18 -5/+4	18 -5/+4	(4)
CPD -59 2628 A	O9.5V	14.0± 20.0	16.5	15.6	18 -5/+4	18 -5/+4	18 -5/+4	18 -5/+4	(4)
LMC									
LMC MACHO 053441.3 A	O3If	41.2± 12.0	66.9	67.5	81 -10/+9	72 -8/+9	82 -10/+6	76 -5/+7	(4)
LMC MACHO 053441.3 B	O6V	27.0± 12.0	31.7	31.0	37 -5/+3	36 -4/+3	37 -5/+3	36 -4/+3	(4)
LMC R136-38 A	O3V	56.9± 6.0	58.3	58.0	64 -7/+7	64 -7/+7	64 -7/+7	64 -7/+7	(4)
LMC R136-38 B	O6V	23.4± 2.0	31.7	31.0	37 -5/+3	36 -4/+3	37 -5/+3	36 -4/+3	(4)
LMC R136-42 A	O3V	40.3± 1.0	58.3	58.0	64 -7/+7	64 -7/+7	64 -7/+7	64 -7/+7	(4)
LMC R136-42 B	O3V	32.6± 1.0	58.3	58.0	64 -7/+7	64 -7/+7	64 -7/+7	64 -7/+7	(4)
LH 54-425 A	O3V	50.0± 10.0	58.3	58.0	64 -7/+7	64 -7/+7	64 -7/+7	64 -7/+7	(9)
LH 54-425 B	O5V	30.0± 6.0	37.3	38.1	44 -5/+5	44 -5/+5	44 -5/+4	43 -4/+5	(9)
LMC R136-77 A	O5.5V	28.9± 3.0	34.2	34.4	40 -5/+4	40 -5/+4	40 -5/+4	39 -4/+4	(4)
LMC R136-77 B	O5.5V	26.2± 3.0	34.2	34.4	40 -5/+4	40 -5/+4	40 -5/+4	39 -4/+4	(4)
LMC-SC1-105 A	O7V	30.9± 1.0	26.5	25.3	31 -5/+3	30 -4/+3	31 -5/+3	30 -4/+3	(10)

Notes. For these massive stars dynamical mass estimates, m_{dyn} , exist from the orbits of binaries. The other mass estimates are from the theoretical T_{eff} calibration (m_{MSH1}) and observational T_{eff} calibration (m_{MSH2}) by MSH05, together with the initial (m_{ini}), mean evolutionary (m_{evol}), minimal (m_{start}) and maximal (m_{end}) present-day mass from this work. The horizontal lines separates objects in the LMC from Galactic ones. All masses are in M_{\odot} . For the Milky Way stars Table 4 was used to derive the masses and for the LMC stars Table 6. ^(a) Different luminosity class determinations exist in the literature. The most recent one was used. ^(b) Error assumed as none given. ^(c) Luminosity class V was assumed.

References. 1: Morrell et al. (2001); Gies (2003), 2: Niemela et al. (2006), 3: Kraus et al. (2009), 4: Gies (2003), 5: Fernández Lajús & Niemela (2006), 6: Mayer et al. (2008), 7: Mayer et al. (2005), 8: Schweickhardt et al. (1999), 9: Williams et al. (2008), 10: Bonanos (2009)

reached during stellar evolution from the hot end by more massive stars and the cold end by less massive stars. This results in a larger range of possible masses. Also, the subtypes are not of the same area in the $L-T_{\text{eff}}$ -space (see Fig. 1). Therefore, some subtypes simply have a higher probability to be encountered by the model tracks. It would be possible to reduce these errors by introducing more luminosity classes, like II, Ia and Ib. But no MSH05 definitions for these classes presently exist.

Furthermore, the table shows the mean time the models spend in each spectral type box. Again, the errors are defined by the lowest and most-massive model passing through the spectral type box, including a ± 1000 K uncertainty for the spectral type definitions. Note that the Meynet & Maeder (2003) models show considerable jumps in T_{eff} and luminosity when the stars enter the Wolf-Rayet phase. These extremely fast crossings (< 50000 years) through the HR-Diagram are not included in the tables.

The newly arrived spectral-type-mass relation, as arrived in Sect. 2, is now compared with the dynamical (Table 2) and literature spectroscopic (Table 3) mass estimates from Sect. 3.

4.1. Comparison with dynamical masses

In Fig. 3 the results of the MSH05 and the present-day mass estimates are compared with dynamical mass estimates for massive stars from the literature as shown in Table 2. Inspecting the mass estimates, a very large spread is noticeable.

The results of a linear correlation analysis for all stars in the sample are shown in Table 8. For each sample, the slope and offset of a best-fitting linear relation are given together with the correlation coefficients. The “MSH1” column provides the mass estimates from MSH05 using the theoretical T_{eff} scale, whilst “MSH2” gives the results from their observational T_{eff} scale. “ini”, “evol”, “start” and “end” are the results arrived at here, with “ini” marking the results for initial masses of the models, “start” the evolved mass when a star enters a spectral type and

Table 3. O-star with spectroscopic mass estimates.

Star	Sp Type	$m_{\text{spectroscopic}}$	m_{MSH1}	m_{MSH2}	m_{evol}
HD93129A ^a	O2If*	94.8 -28.8/+41.3	66.9 ⁺	67.5 ⁺	95 -33/+25
HD14947	O5I	30.7 -9.2/+13.1	50.9	50.7	47 -4/+17
HD210839 ^b	O6I	62.2 -24.9/+41.5	45.8	44.1	42 -3/+15
HD192639	O7I	37.5 -11.2/+16.1	40.9	38.4	39 -5/+24
HD193514	O7I	28.2 -8.5/+12.1	40.9	38.4	39 -5/+24
HD210809	O9I	21.7 -6.6/+9.4	32.0	29.6	33 -5/+11
HD207198 ^a	O9I	29.0 -8.7/+12.5	32.0	29.6	33 -5/+11
HD30614	O9.5I	37.6 -11.2/+16.1	30.4	27.8	32 -5/+13
HD209975 ^a	O9.5I	31.4 -9.4/+13.4	30.4	27.8	32 -5/+13
HD15558 ^a	O5III	78.7 -23.7/+33.8	41.5	40.4	47 -5/+6
HD193682	O5III	27.9 -8.2/+11.7	41.5	40.4	47 -5/+6
HD190864	O6.5III	20.3 -6.1/+8.7	33.7	32.0	36 -4/+5
HD24912	O7.5III	26.1 -7.6/+10.9	29.1	27.5	31 -4/+5
HD203064	O7.5III	35.9 10.3/+14.9	29.1	27.5	31 -4/+5
HD191423 ^c	O9III	24.6 -7.0/+11.2	23.1	22.0	26 -4/+5
HD93128	O3V	39.8 -12.0/+17.2	58.3	58.0	65 -7/+8
HD93250	O3V	83.3 -25.1/+36.0	58.3	58.0	65 -7/+8
HD66811	O4V	53.9 -19.5/+30.8	46.2	46.9	54 -6/+7
HD15629 ^a	O5V	30.4 -9.1/+13.1	37.3	38.1	44 -6/+7
HD217086	O7V	14.2 -4.0/+6.3	26.5	25.3	27 -5/+7
HD149757 ^b	O9V	20.2 -5.7/+8.8	18.0	17.1	19 -5/+5

Notes. Mass estimates arrived at by spectral line fitting ($m_{\text{spectroscopic}}$) from Repolust et al. (2004). Additionally, the mass estimates from MSH05 (m_{MSH1} and m_{MSH2}) and this work (m_{evol}) are shown. All masses are in M_{\odot} . ^(a) Member of a binary system. ^(b) Runaway star. ^(c) Extremely fast rotator.

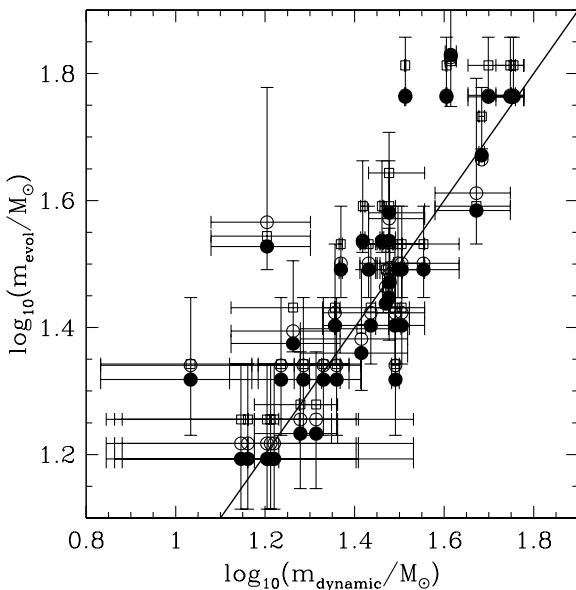


Fig. 3. Comparison of the different mass estimates with dynamically determined stellar masses. The *solid line* marks a one-to-one correspondence between model and dynamical mass. *Open circles* show the masses for the MSH05 theoretical O star T_{eff} scale, *closed circles* for the MSH05 observational temperature scale and *open boxes* mark the mean masses derived in this work.

“end” the one when he leaves it. “Evol” is the mean mass computed from m_{start} and m_{end} . With an offset very close to 0, a slope of nearly 1, and a correlation coefficient of ~ 0.9 , the MSH05 mass estimates agree very well with the dynamical masses of

the sample. Furthermore, the minimal, maximal, and evolutionary present-day masses, which are calibrated on the theoretical T_{eff} scale of MSH05, agree very well with the observed dynamical masses. The offsets are quite close to 0 and slopes similarly close to 1, whilst the correlation coefficients are ~ 0.9 too. The present-day dynamical masses are therefore quite well reproduced by the models. Note that the errors for the MSH05 based fits are always smaller than the fits with the here-derived values. This is because the MSH05 values involve no errors, and the fit only contains errors in the dynamical masses. The values derived here values also have their own error estimate.

In Figs. 4 to 6 the dynamical masses from Table 2 (open circles) are shown together with the present-day mass range (m_{start} to m_{end}) for the models (shaded region), for the supergiants (Fig. 4), giants (Fig. 5) and dwarfs (Fig. 6). Evidently, most of the dynamical measurements agree well with the models within the error bars. For supergiants and giants the mass ranges for different metallicities are nearly indistinguishable. Only the non-rotating evolutionary models stand out in the case of the supergiants. Because the dependence of mass loss on rotation is not understood very well, this discrepancy is likely very dependent on the assumptions in the stellar evolutionary code. For dwarf stars only the SMC metallicity mass ranges differ visibly from the solar and LMC estimates. Somewhat surprisingly, the early-type SMC dwarfs seem to have *lower* masses than their MW and LMC cousins, according to the models and definitions used here. This is almost certainly because of the earlier mentioned perhaps unexpected fact that the Heap et al. (2006) SMC O stars result in a lower T_{eff} scale for O stars than for LMC objects.

Interestingly, all but two of the (dwarf) stars located in the LMC (*en-circled circles* in Fig. 6) lie below the here derived solar and LMC metallicity evolutionary mass ranges, independent of rotation and metallicity. Only the allowed mass range for SMC metallicity covers these stars.

This might be because of binary stellar evolution because it is more difficult to access if the stars are detached or not in the LMC. The lower metallicity of the LMC might also not be ac-

Table 4. Theoretical masses for O stars from rotating stellar models.

Spectral type	m_{ini} M_{\odot}	m_{evol} M_{\odot}	m_{start} M_{\odot}	m_{end} M_{\odot}	$t_{\text{start,min}}$ Myr	$t_{\text{start,max}}$ Myr	$t_{\text{end,min}}$ Myr	$t_{\text{end,max}}$ Myr
O 2.0 If*	107 -27/+13	95 -33/+25	107 -45/+13	83 -21/+11	0.0	1.5	0.1	1.8
O 2.0 I	95 -18/+22	79 -19/+15	84 -24/+10	75 -14/+11	0.9	1.8	1.2	2.0
O 2.5 I	86 -14/+27	72 -14/+14	76 -18/+9	67 -9/+16	1.2	2.1	1.4	2.3
O 3.0 I	79 -10/+29	66 -10/+16	69 -12/+12	62 -7/+18	1.4	2.5	1.6	2.5
O 3.5 I	72 -8/+31	60 -8/+18	62 -10/+15	58 -5/+20	1.6	2.4	1.9	2.5
O 4.0 I	66 -7/+31	55 -9/+19	57 -7/+17	54 -7/+21	1.9	2.8	2.2	2.8
O 4.5 I	60 -4/+33	50 -5/+23	52 -6/+20	47 -3/+24	2.2	2.9	2.5	3.1
O 5.0 I	57 -5/+26	47 -4/+17	48 -5/+15	45 -2/+18	2.6	3.2	2.9	3.4
O 5.5 I	54 -6/+23	44 -3/+16	45 -4/+14	43 -2/+17	2.9	3.9	3.2	4.0
O 6.0 I	51 -6/+21	42 -3/+15	43 -4/+14	41 -2/+16	3.3	4.1	3.6	4.2
O 6.5 I	47 -6/+26	39 -3/+18	40 -4/+17	39 -3/+18	3.6	4.3	3.9	4.5
O 7.0 I	47 -9/+36	39 -5/+24	40 -6/+23	39 -5/+24	3.8	4.7	4.1	4.7
O 7.5 I	43 -7/+39	37 -4/+26	37 -5/+25	36 -4/+26	4.2	5.1	4.5	5.1
O 8.0 I	42 -7/+38	35 -4/+26	36 -5/+24	35 -3/+26	4.6	5.3	4.7	5.4
O 8.5 I	40 -7/+41	33 -4/+25	34 -4/+25	33 -3/+11	4.7	5.7	4.8	5.7
O 9.0 I	40 -9/+43	33 -5/+11	33 -5/+11	33 -4/+11	4.9	6.0	4.9	6.0
O 9.5 I	37 -8/+47	32 -5/+13	32 -5/+12	31 -5/+13	5.0	6.4	5.1	6.4
O 2.0 III	86 -12/+7	77 -18/+12	78 -19/+11	76 -17/+11	0.6	1.4	0.7	1.8
O 2.5 III	79 -10/+7	71 -14/+9	73 -16/+7	69 -12/+11	0.8	1.8	1.0	2.1
O 3.0 III	73 -8/+7	65 -11/+8	68 -13/+6	62 -8/+11	1.0	2.1	1.2	2.5
O 3.5 III	67 -7/+8	60 -8/+8	62 -7/+6	58 -6/+10	1.1	2.8	1.3	2.8
O 4.0 III	62 -6/+8	56 -6/+8	57 -5/+6	54 -5/+8	1.2	2.7	1.4	3.0
O 4.5 III	57 -6/+7	51 -4/+7	52 -5/+5	50 -3/+7	1.4	2.9	1.7	3.2
O 5.0 III	52 -6/+7	47 -5/+6	48 -6/+4	46 -4/+6	1.6	3.2	2.0	3.6
O 5.5 III	47 -7/+8	43 -5/+6	44 -6/+5	42 -4/+6	1.9	3.5	2.4	3.9
O 6.0 III	43 -6/+7	39 -4/+6	39 -5/+5	39 -4/+5	2.4	3.8	2.8	4.1
O 6.5 III	39 -5/+7	36 -4/+5	37 -4/+5	36 -4/+5	2.8	4.1	3.4	4.3
O 7.0 III	36 -5/+7	34 -4/+6	34 -4/+5	33 -4/+5	3.2	4.6	3.7	4.7
O 7.5 III	33 -5/+6	31 -4/+5	31 -5/+4	31 -4/+5	3.7	5.0	4.1	5.2
O 8.0 III	31 -6/+6	29 -5/+5	29 -5/+5	29 -5/+5	4.1	5.5	4.5	5.6
O 8.5 III	29 -5/+6	27 -4/+5	27 -4/+5	27 -4/+5	4.5	5.9	4.9	6.1
O 9.0 III	27 -5/+6	26 -4/+5	26 -4/+5	26 -4/+5	5.1	6.6	5.3	6.7
O 9.5 III	26 -5/+5	24 -4/+5	24 -4/+4	24 -4/+4	5.5	7.1	5.7	7.3
O 2.0 V	86 -11/+8	83 -23/+9	85 -25/+8	81 -21/+11	0.0	1.1	0.1	1.3
O 2.5 V	76 -12/+7	73 -10/+7	75 -11/+6	71 -8/+8	0.0	1.0	0.1	1.5
O 3.0 V	67 -9/+9	65 -7/+8	67 -9/+6	64 -6/+9	0.0	1.4	0.1	1.8
O 3.5 V	61 -8/+8	59 -6/+7	60 -7/+6	58 -5/+8	0.0	1.8	0.1	1.9
O 4.0 V	56 -8/+7	54 -6/+7	55 -7/+5	53 -5/+7	0.0	1.7	0.1	2.1
O 4.5 V	51 -8/+6	49 -6/+6	50 -7/+5	49 -6/+6	0.0	2.0	0.1	2.4
O 5.0 V	45 -7/+8	44 -6/+7	45 -7/+6	43 -5/+7	0.0	2.2	0.1	2.7
O 5.5 V	40 -7/+8	39 -6/+7	39 -6/+6	38 -5/+7	0.0	2.6	0.1	3.1
O 6.0 V	35 -7/+6	34 -6/+6	34 -6/+5	33 -6/+6	0.0	3.1	0.2	3.6
O 6.5 V	31 -7/+6	30 -6/+6	30 -6/+5	30 -6/+6	0.0	3.6	0.1	4.1
O 7.0 V	28 -6/+8	27 -5/+7	27 -5/+6	27 -5/+7	0.0	4.1	0.4	4.6
O 7.5 V	25 -5/+7	25 -5/+7	25 -5/+6	25 -5/+6	0.0	4.6	0.3	5.1
O 8.0 V	23 -6/+6	22 -5/+6	22 -5/+6	22 -5/+6	0.0	5.1	0.1	5.5
O 8.5 V	21 -6/+5	21 -6/+5	21 -6/+5	21 -6/+5	0.0	5.5	0.2	6.1
O 9.0 V	19 -5/+5	19 -5/+5	19 -5/+4	19 -5/+4	0.0	6.2	0.2	6.8
O 9.5 V	18 -5/+4	18 -5/+4	18 -5/+4	18 -5/+4	0.0	6.8	0.2	7.5

Notes. Theoretical masses for O stars from rotating solar metallicity stellar evolution models (Meynet & Maeder 2003). The first mass (m_{ini}) denotes the initial mass of the model weighted by the time the star resides in that spectral type. The weighting is done in order to present the most likely mass for a spectral type. The lower and upper mass limit show which range of initial masses can reach a certain spectral type. The mean mass of the star which stays longest in a certain spectral type is denoted by m_{evol} . The third mass (m_{start}) is the mass with which the star starts when entering this spectral type while the fourth mass (m_{end}) is the mass at the end of the stay in that particular spectral type. For each subclass is also given the minimal and maximal age the models when they enter it ($t_{\text{start,min}}, t_{\text{start,max}}$) and when they leave ($t_{\text{end,min}}, t_{\text{end,max}}$).

counted for correctly either in the evolutionary models or in the atmosphere models. The large distance to these stars compared to the rest of the sample might also influence the observed values. However, removing these nine stars from the already small sample of only 30 stars would strongly reduce its significance.

In one case (V1182 Aql A) the initial mass is slightly *above* the dynamical mass for its spectral type, even when considering

the uncertainties in the observational and model mass determination. This might be caused by a somewhat optimistic observational error ($\pm 0.6 M_{\odot}$) or can be because of binary stellar evolution effects such as mass transfer, or excess irradiation of one stellar hemisphere in tidally locked configurations.

Table 5. Theoretical masses for O stars from non-rotating stellar models.

Spectral type	m_{ini} M_{\odot}	m_{evol} M_{\odot}	m_{start} M_{\odot}	m_{end} M_{\odot}	$t_{\text{start,min}}$ Myr	$t_{\text{start,max}}$ Myr	$t_{\text{end,min}}$ Myr	$t_{\text{end,max}}$ Myr
O 2.0 If*	105 -23/+15	101 -19/+19	105 -23/+15	96 -14/+13	0.0	1.0	0.1	1.2
O 2.0 I	103 -17/+17	93 -15/+15	94 -16/+14	93 -15/+15	0.9	1.4	1.1	1.4
O 2.5 I	99 -18/+21	89 -16/+18	90 -16/+17	89 -15/+18	1.1	1.5	1.2	1.6
O 3.0 I	97 -21/+23	86 -18/+20	87 -18/+19	86 -17/+19	1.2	1.7	1.3	1.7
O 3.5 I	96 -24/+24	84 -19/+21	84 -19/+20	83 -19/+20	1.3	1.8	1.4	1.9
O 4.0 I	94 -27/+26	81 -21/+22	82 -21/+21	81 -21/+21	1.4	2.0	1.5	2.0
O 4.5 I	91 -29/+29	78 -22/+24	79 -23/+23	78 -22/+22	1.5	2.2	1.6	2.3
O 5.0 I	78 -20/+42	68 -16/+32	68 -16/+31	68 -15/+31	1.7	2.5	1.7	2.5
O 5.5 I	68 -14/+49	60 -11/+37	60 -11/+36	60 -11/+36	1.7	2.7	1.8	2.8
O 6.0 I	66 -16/+19	58 -13/+15	58 -13/+14	58 -12/+15	2.1	3.0	2.1	3.0
O 6.5 I	64 -18/+21	56 -14/+17	56 -14/+16	56 -14/+16	2.2	3.3	2.2	3.3
O 7.0 I	61 -20/+24	53 -16/+18	54 -16/+18	53 -15/+18	2.3	3.7	2.3	3.7
O 7.5 I	53 -14/+32	47 -11/+24	47 -11/+24	47 -11/+24	2.3	3.9	2.3	4.0
O 8.0 I	48 -11/+35	43 -9/+27	43 -8/+26	43 -9/+26	2.4	4.3	2.4	4.3
O 8.5 I	46 -10/+35	41 -8/+27	42 -8/+26	41 -8/+27	2.5	4.4	2.5	4.5
O 9.0 I	45 -11/+15	40 -9/+12	41 -9/+11	40 -8/+11	3.1	4.8	3.1	4.8
O 9.5 I	44 -13/+16	38 -8/+15	40 -10/+12	36 -7/+14	3.1	5.3	3.2	5.4
O 2.0 III	88 -5/+6	82 -6/+7	83 -6/+6	82 -5/+7	0.6	1.2	0.8	1.4
O 2.5 III	81 -5/+6	75 -5/+6	76 -5/+5	74 -4/+7	0.8	1.4	1.0	1.5
O 3.0 III	74 -6/+7	69 -6/+7	70 -7/+6	68 -5/+7	1.0	1.6	1.2	1.7
O 3.5 III	69 -7/+7	64 -6/+7	64 -6/+6	63 -6/+7	1.1	1.7	1.3	1.9
O 4.0 III	64 -7/+8	59 -6/+8	59 -6/+7	58 -5/+8	1.3	1.9	1.4	2.1
O 4.5 III	59 -7/+8	54 -6/+8	55 -6/+7	54 -5/+7	1.4	2.1	1.6	2.3
O 5.0 III	54 -6/+9	50 -5/+8	51 -5/+7	50 -5/+8	1.6	2.4	1.9	2.6
O 5.5 III	49 -8/+9	45 -7/+8	46 -7/+7	45 -6/+8	1.9	2.8	2.2	2.9
O 6.0 III	44 -6/+10	41 -5/+9	42 -5/+8	41 -5/+8	2.3	3.2	2.5	3.3
O 6.5 III	41 -6/+9	38 -5/+8	39 -5/+7	38 -5/+7	2.7	3.6	2.8	3.7
O 7.0 III	38 -6/+8	36 -5/+7	36 -5/+7	36 -5/+7	3.1	4.1	3.1	4.1
O 7.5 III	34 -5/+8	33 -5/+7	33 -5/+6	33 -5/+6	3.4	4.5	3.4	4.6
O 8.0 III	32 -6/+7	30 -5/+7	30 -5/+6	30 -5/+6	3.7	5.0	3.7	5.1
O 8.5 III	30 -6/+7	28 -5/+7	28 -5/+6	28 -5/+6	4.0	5.5	4.0	5.6
O 9.0 III	28 -5/+7	27 -4/+6	27 -4/+6	27 -4/+6	4.3	5.9	4.4	6.0
O 9.5 III	27 -6/+6	26 -5/+6	26 -5/+5	26 -5/+5	4.6	6.7	4.7	6.7
O 2.0 V	85 -11/+8	82 -9/+8	84 -10/+7	81 -7/+9	0.0	1.0	0.1	1.2
O 2.5 V	74 -13/+9	72 -11/+8	74 -13/+6	71 -10/+8	0.0	1.1	0.1	1.4
O 3.0 V	66 -10/+10	64 -8/+9	65 -9/+7	63 -7/+9	0.0	1.4	0.1	1.6
O 3.5 V	60 -9/+9	58 -7/+8	59 -8/+7	57 -6/+8	0.0	1.5	0.1	1.7
O 4.0 V	54 -8/+9	53 -7/+8	53 -7/+7	52 -6/+8	0.0	1.7	0.1	1.9
O 4.5 V	49 -8/+8	48 -7/+7	49 -8/+6	48 -7/+7	0.0	1.9	0.1	2.1
O 5.0 V	44 -7/+9	43 -6/+8	44 -7/+7	42 -6/+8	0.0	2.1	0.1	2.4
O 5.5 V	39 -7/+9	38 -6/+8	39 -7/+7	38 -6/+8	0.0	2.4	0.1	2.8
O 6.0 V	34 -8/+8	33 -7/+8	33 -7/+7	33 -7/+7	0.0	2.9	0.1	3.3
O 6.5 V	30 -7/+8	29 -6/+8	29 -6/+7	29 -6/+7	0.0	3.3	0.1	3.7
O 7.0 V	27 -6/+8	26 -5/+8	26 -5/+7	26 -5/+7	0.0	3.7	0.2	4.2
O 7.5 V	24 -5/+8	24 -5/+7	24 -5/+7	24 -5/+7	0.0	4.2	0.1	4.6
O 8.0 V	22 -5/+7	22 -5/+7	22 -5/+6	22 -5/+6	0.0	4.7	0.2	5.2
O 8.5 V	20 -5/+6	20 -5/+6	20 -5/+5	20 -5/+5	0.0	5.2	0.2	5.7
O 9.0 V	19 -5/+5	19 -5/+5	19 -5/+5	19 -5/+5	0.0	5.7	0.2	6.4
O 9.5 V	17 -4/+5	17 -4/+5	17 -4/+4	17 -4/+4	0.0	6.4	0.2	7.2

4.2. Comparison with spectroscopic masses

Spectroscopic mass determinations are the only other empirical method to derive stellar masses for single stars and non-eclipsing binaries. The hot and usually rapidly-rotating O stars have very broad spectral features, which often result in large error bars from the line-fitting techniques used to fit model spectra to observations. The literature spectroscopic mass values from Repolust et al. (2004) are shown in Table 3 and are also plotted in Figs. 4 to 6 as *filled circles*. The spread seems to be somewhat larger than the spread of the dynamical mass estimates and it should be noted that several (3 out of 21) of the spectroscopic measurements are so far outside the predictions that the error bars do not overlap. Two of these three stars are giants

(HD190864 and HD193682) and one is a dwarf (HD217086). Reassuringly, all supergiants (Fig. 4) overlap at least with their error bars with the model predictions, and apart from the mentioned exceptions all giants and dwarfs, too.

The large spread and the three outlying stars might be because of the generally much larger errors of the spectroscopic masses determinations compared to dynamical ones. Heap et al. (2006) find in their study of SMC stars that the mass discrepancy is reduced but not eliminated when using NLTE line-blanketed model atmospheres. They suggest that the remaining difference is actually a signature of fast rotation that would lower the apparent surface gravity. As also indicated in Table 3, some of the stars are known binaries and two runaway stars are also included

Table 6. Theoretical masses for O stars from rotating LMC ($z=0.008$) stellar models.

Spectral type	m_{ini} M_{\odot}	m_{evol} M_{\odot}	m_{start} M_{\odot}	m_{end} M_{\odot}	$t_{\text{start,min}}$ Myr	$t_{\text{start,max}}$ Myr	$t_{\text{end,min}}$ Myr	$t_{\text{end,max}}$ Myr
O 2.0 If*	107 -25/+13	100 -18/+19	107 -25/+13	94 -12/+10	0.0	2.4	0.1	2.5
O 2.0 I	96 -10/+10	86 -10/+10	90 -10/+6	82 -6/+11	0.8	2.5	1.1	2.7
O 2.5 I	88 -10/+9	79 -8/+9	82 -10/+6	76 -5/+7	1.0	2.7	1.1	2.8
O 3.0 I	81 -11/+10	72 -8/+9	75 -10/+6	70 -6/+7	1.3	3.0	1.3	3.0
O 3.5 I	74 -11/+12	66 -8/+8	68 -9/+6	64 -6/+8	1.6	3.1	1.9	3.1
O 4.0 I	67 -9/+13	60 -7/+8	61 -7/+7	59 -6/+8	1.9	3.2	2.0	3.2
O 4.5 I	62 -8/+16	56 -6/+10	57 -7/+9	55 -5/+10	2.3	3.2	2.5	3.3
O 5.0 I	58 -8/+20	52 -6/+14	53 -6/+13	52 -6/+14	2.5	3.6	2.8	3.7
O 5.5 I	55 -9/+22	49 -7/+16	50 -7/+15	49 -6/+16	2.8	4.0	2.8	4.0
O 6.0 I	52 -9/+25	47 -7/+19	47 -7/+18	46 -6/+18	3.1	4.0	3.1	4.1
O 6.5 I	49 -10/+28	44 -7/+21	44 -7/+21	43 -7/+21	3.1	4.3	3.1	4.4
O 7.0 I	46 -9/+30	41 -7/+23	42 -7/+22	41 -6/+23	3.1	4.7	3.2	4.7
O 7.5 I	43 -8/+12	39 -6/+8	40 -7/+7	39 -6/+8	4.2	5.0	4.2	5.1
O 8.0 I	41 -9/+12	38 -7/+8	38 -7/+8	37 -7/+8	4.4	5.5	4.4	5.5
O 8.5 I	39 -9/+13	36 -7/+9	36 -7/+9	36 -7/+9	4.5	5.9	4.6	5.9
O 9.0 I	37 -8/+14	34 -6/+10	34 -7/+9	34 -6/+10	4.6	6.2	4.7	6.3
O 9.5 I	37 -10/+13	33 -7/+10	34 -8/+9	33 -7/+10	4.8	7.4	4.8	7.4
O 2.0 III	87 -10/+10	84 -9/+10	86 -10/+8	83 -7/+11	0.0	1.5	0.1	1.7
O 2.5 III	78 -10/+12	76 -9/+11	77 -11/+9	75 -8/+12	0.0	1.8	0.1	2.0
O 3.0 III	70 -10/+12	67 -9/+12	69 -10/+10	66 -8/+12	0.1	2.2	0.4	2.2
O 3.5 III	62 -7/+12	60 -6/+11	61 -7/+9	59 -5/+11	0.2	2.2	0.6	2.5
O 4.0 III	57 -6/+9	54 -5/+9	55 -5/+7	54 -4/+9	0.5	2.5	1.1	2.8
O 4.5 III	52 -5/+7	50 -5/+7	50 -5/+5	49 -4/+6	0.8	2.8	1.1	3.0
O 5.0 III	48 -6/+7	46 -5/+7	46 -5/+6	45 -5/+6	1.1	3.4	1.6	3.4
O 5.5 III	44 -5/+7	42 -4/+7	42 -4/+6	41 -4/+7	1.6	3.7	1.6	3.7
O 6.0 III	40 -4/+8	39 -4/+7	39 -4/+6	38 -4/+7	1.9	3.9	2.5	4.0
O 6.5 III	37 -4/+7	36 -4/+7	36 -4/+6	35 -3/+6	2.4	4.3	3.0	4.4
O 7.0 III	34 -4/+5	33 -4/+5	33 -4/+4	33 -3/+4	2.9	4.4	3.2	4.8
O 7.5 III	32 -4/+6	31 -3/+6	31 -3/+5	31 -3/+6	3.4	4.9	3.5	5.3
O 8.0 III	30 -4/+5	29 -3/+5	29 -3/+5	29 -3/+5	3.8	5.4	4.7	5.9
O 8.5 III	28 -4/+5	27 -3/+5	27 -4/+5	27 -3/+5	4.4	6.1	5.0	6.4
O 9.0 III	25 -3/+5	25 -3/+5	25 -3/+4	25 -3/+4	5.4	7.1	5.5	7.1
O 9.5 III	23 -2/+5	23 -2/+5	23 -2/+4	23 -2/+4	5.8	7.2	6.2	7.7
O 2.0 V	80 -8/+6	80 -8/+5	80 -8/+5	80 -8/+5	0.0	0.1	0.1	0.4
O 2.5 V	72 -9/+6	72 -9/+6	72 -9/+5	72 -9/+6	0.0	0.4	0.1	0.8
O 3.0 V	64 -7/+7	64 -7/+7	64 -7/+7	64 -7/+7	0.0	0.8	0.1	1.1
O 3.5 V	58 -5/+6	57 -5/+6	58 -5/+6	57 -4/+7	0.0	0.8	0.1	1.4
O 4.0 V	53 -5/+4	53 -5/+4	53 -5/+4	52 -5/+4	0.0	1.2	0.1	1.7
O 4.5 V	49 -6/+4	48 -5/+4	49 -6/+4	48 -5/+4	0.0	2.0	0.1	2.0
O 5.0 V	44 -5/+5	44 -5/+5	44 -5/+4	43 -4/+5	0.0	2.0	0.1	2.5
O 5.5 V	40 -5/+4	40 -5/+4	40 -5/+4	39 -4/+4	0.0	2.1	0.1	2.8
O 6.0 V	37 -5/+3	36 -4/+3	37 -5/+3	36 -4/+3	0.0	3.0	0.1	3.2
O 6.5 V	34 -5/+3	33 -4/+3	33 -4/+3	33 -4/+3	0.0	3.4	0.1	3.7
O 7.0 V	31 -5/+3	30 -4/+3	31 -5/+3	30 -4/+3	0.0	3.6	0.1	4.2
O 7.5 V	28 -5/+3	28 -5/+3	28 -5/+3	27 -4/+3	0.0	4.2	0.2	4.8
O 8.0 V	25 -4/+4	25 -4/+4	25 -4/+3	25 -4/+4	0.0	4.3	0.1	5.4
O 8.5 V	22 -4/+5	22 -4/+5	22 -4/+4	22 -4/+4	0.0	5.8	0.2	6.1
O 9.0 V	20 -4/+4	20 -4/+4	20 -4/+4	20 -4/+3	0.0	6.7	0.1	6.8
O 9.5 V	18 -2/+5	18 -2/+5	18 -2/+4	18 -2/+4	0.0	6.7	0.1	7.5

in the sample, though these stars agree reasonably well with the models. For such objects binary stellar evolution could have strongly influenced the present-day mass, and/or spectrum of the star. Nonetheless, the evolutionary model based spectral-type–mass-relation derived here agrees with dynamical as well as spectroscopic mass estimates, suggesting the systematic mass-discrepancy problem might be solved.

5. Summary and conclusions

With the spectral type definition of MSH05, a relation between O star spectral type and its mass and age was derived for solar metallicity stars. This was achieved by taking stellar evolu-

tion models (Meynet & Maeder 2003) and comparing their output luminosities and T_{eff} with the MSH05 spectral type definitions. With the Mokiem et al. (2007) study of O stars in the LMC, the Heap et al. (2006) data for SMC O stars and evolutionary tracks by Meynet & Maeder (2005) and Bertelli et al. (2009), similar spectral-type–mass-relations were derived for LMC and SMC metallicity. The resulting mass versus spectral-type relation agrees well with dynamical as well as spectroscopic mass measurements from the literature for MW and LMC main-sequence stars. For SMC stars, giants and supergiants too few or no dynamical mass estimates are available for an in-depth comparison.

Table 7. Theoretical masses for O stars from rotating SMC ($z=0.004$) stellar models.

Spectral type	m_{ini} M_{\odot}	m_{evol} M_{\odot}	m_{start} M_{\odot}	m_{end} M_{\odot}	$t_{\text{start,min}}$ Myr	$t_{\text{start,max}}$ Myr	$t_{\text{end,min}}$ Myr	$t_{\text{end,max}}$ Myr
O 2.0 If*	90 -39/+30	86 -35/+34	90 -39/+30	82 -31/+26	0.0	2.5	0.1	2.5
O 2.0 I	97 -20/+23	86 -17/+21	87 -17/+20	86 -16/+20	2.4	2.6	2.4	2.7
O 2.5 I	87 -17/+22	78 -14/+18	79 -15/+17	77 -13/+18	2.6	2.8	2.8	2.9
O 3.0 I	80 -16/+19	72 -13/+15	72 -13/+14	71 -12/+15	2.8	3.0	2.9	3.1
O 3.5 I	75 -16/+18	67 -12/+14	67 -13/+13	67 -12/+14	3.0	3.1	3.1	3.2
O 4.0 I	70 -15/+18	63 -12/+14	63 -12/+13	62 -11/+14	3.1	3.3	3.2	3.4
O 4.5 I	65 -13/+18	59 -11/+13	59 -11/+12	59 -10/+13	3.3	3.5	3.3	3.6
O 5.0 I	61 -13/+19	55 -10/+14	55 -10/+14	55 -10/+14	3.4	3.8	3.4	3.8
O 5.5 I	56 -11/+23	51 -9/+17	52 -9/+16	51 -9/+17	3.4	4.0	3.4	4.1
O 6.0 I	53 -12/+26	49 -10/+20	49 -10/+19	49 -10/+19	3.4	4.3	3.4	4.4
O 6.5 I	51 -12/+27	47 -10/+21	47 -10/+20	47 -10/+20	3.4	4.6	3.4	4.6
O 7.0 I	50 -12/+28	45 -9/+22	46 -9/+21	45 -9/+22	3.5	4.9	3.5	4.9
O 7.5 I	47 -11/+30	43 -9/+23	44 -9/+23	43 -9/+23	3.5	5.3	3.5	5.3
O 8.0 I	46 -12/+14	42 -10/+11	42 -10/+11	42 -10/+11	4.2	5.5	4.2	5.6
O 8.5 I	44 -12/+16	40 -10/+12	41 -10/+12	40 -10/+12	4.3	5.9	4.3	6.0
O 9.0 I	44 -13/+16	40 -11/+13	40 -11/+12	40 -11/+12	4.3	6.4	4.3	6.4
O 9.5 I	41 -12/+18	38 -10/+14	38 -10/+14	38 -10/+14	4.6	6.8	4.6	6.8
O 2.0 III	71 -11/+17	67 -10/+15	67 -10/+14	66 -9/+15	2.0	2.5	2.0	2.6
O 2.5 III	65 -9/+15	61 -8/+13	61 -8/+13	61 -7/+13	2.2	2.8	2.3	2.8
O 3.0 III	60 -7/+13	57 -6/+11	57 -6/+11	56 -6/+11	2.4	2.8	2.7	3.0
O 3.5 III	56 -7/+10	53 -6/+9	53 -6/+9	52 -6/+9	2.6	3.0	2.8	3.2
O 4.0 III	52 -7/+7	49 -6/+7	49 -6/+6	49 -6/+7	2.9	3.4	3.1	3.4
O 4.5 III	48 -6/+8	46 -5/+7	46 -5/+7	46 -5/+7	3.2	3.5	3.3	3.7
O 5.0 III	45 -6/+8	43 -5/+8	43 -5/+7	42 -5/+7	3.5	3.7	3.5	3.9
O 5.5 III	42 -4/+7	40 -4/+7	40 -4/+6	40 -3/+6	3.8	4.0	3.9	4.2
O 6.0 III	39 -3/+6	38 -3/+5	38 -3/+5	38 -3/+5	4.1	4.4	4.1	4.5
O 6.5 III	37 -3/+5	36 -3/+5	36 -3/+4	35 -3/+5	4.4	4.8	4.4	4.9
O 7.0 III	35 -3/+4	34 -3/+4	34 -3/+3	34 -3/+4	4.7	5.2	4.7	5.2
O 7.5 III	33 -4/+4	32 -3/+4	32 -3/+3	32 -3/+3	5.0	5.4	5.1	5.6
O 8.0 III	32 -4/+4	30 -3/+4	30 -3/+4	30 -3/+4	5.4	5.9	5.5	6.1
O 8.5 III	30 -4/+4	29 -4/+4	29 -4/+4	29 -4/+4	5.7	6.4	5.7	6.5
O 9.0 III	28 -2/+4	27 -2/+4	27 -2/+3	27 -2/+3	6.1	6.6	6.1	6.9
O 9.5 III	27 -7/+4	26 -6/+4	26 -6/+4	26 -6/+4	6.5	7.4	6.6	7.5
O 2.0 V	57 -10/+13	56 -9/+12	56 -9/+11	56 -9/+12	0.0	1.9	0.1	2.2
O 2.5 V	52 -8/+10	51 -8/+9	52 -8/+8	51 -7/+9	0.0	2.2	0.1	2.4
O 3.0 V	48 -8/+9	48 -8/+8	48 -8/+7	47 -7/+8	0.0	2.6	0.1	2.6
O 3.5 V	45 -7/+9	44 -6/+9	44 -6/+8	44 -6/+9	0.0	2.7	0.1	2.9
O 4.0 V	42 -6/+8	41 -5/+8	41 -5/+7	41 -5/+8	0.0	2.8	0.1	3.1
O 4.5 V	39 -6/+8	38 -5/+8	38 -5/+7	38 -5/+8	0.0	3.1	0.2	3.4
O 5.0 V	36 -5/+7	35 -5/+7	36 -5/+6	35 -4/+6	0.0	3.5	0.3	3.7
O 5.5 V	34 -6/+5	33 -5/+5	33 -5/+5	33 -5/+5	0.0	4.0	0.1	4.1
O 6.0 V	31 -5/+7	31 -5/+7	31 -5/+6	31 -5/+6	0.0	4.1	0.3	4.4
O 6.5 V	29 -5/+7	29 -5/+7	29 -5/+6	28 -5/+6	0.0	4.4	0.5	4.8
O 7.0 V	27 -6/+7	26 -6/+7	26 -6/+7	26 -5/+7	0.0	5.2	0.5	5.2
O 7.5 V	24 -5/+8	23 -5/+8	23 -5/+8	23 -5/+8	0.0	5.2	0.1	5.6
O 8.0 V	21 -4/+8	21 -4/+8	21 -4/+8	21 -3/+8	0.0	5.6	1.7	6.1
O 8.5 V	20 -4/+8	19 -4/+8	20 -4/+8	19 -4/+8	0.0	6.1	0.2	6.7
O 9.0 V	18 -3/+9	18 -3/+9	18 -3/+8	18 -3/+8	0.0	6.7	0.9	7.4
O 9.5 V	16 -3/+7	16 -3/+7	16 -3/+7	16 -3/+7	0.0	7.4	0.1	8.3

Table 8. Correlation function values.

Value	m_{MSH1}	m_{MSH2}	m_{ini}	m_{evol}	m_{start}	m_{end}
offset	0.017 ± 0.300	-0.051 ± 0.311	0.016 ± 0.308	0.052 ± 0.296	0.027 ± 0.295	0.053 ± 0.269
slope	1.010 ± 0.207	1.048 ± 0.214	1.043 ± 0.216	1.001 ± 0.206	1.029 ± 0.209	1.008 ± 0.208
corr. coeff.	0.887 ± 0.118	0.879 ± 0.115	0.871 ± 0.184	0.858 ± 0.174	0.854 ± 0.170	0.855 ± 0.173

Tables 4 and 5 provide easy access to the mass estimates for a given spectral type based on rotating (Table 4) and non-rotating (Table 5) solar metallicity O star models. Tables 6 and 7 provide the same for LMC and SMC metallicity.

Furthermore, the evolution of individual stellar models (Meynet & Maeder 2003, 2005; Bertelli et al. 2009) through the different spectral types are given in appendix B. For the $z =$

0.02 and 0.04 the MSH05 solar metallicity definitions of spectral types are used, while for $z = 0.008$ the LMC ones and for $z = 0.004$ the SMC ones.

The new calibration of O star spectral types presented here with stellar evolution models provides a valuable new tool to derive O star masses, including initial and present-day masses, and includes an estimate of the errors. Furthermore, the minimal

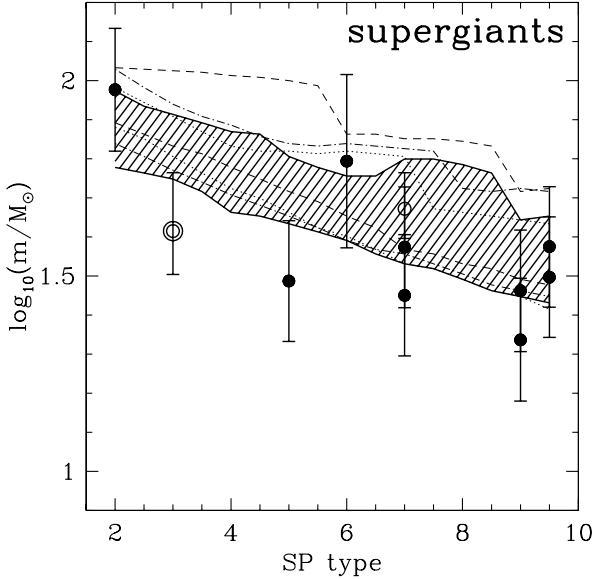


Fig. 4. Comparison of the dynamical (open circles) and spectroscopic (filled circles) mass measurements for luminosity class I objects (supergiants) with the evolutionary masses. The shaded region between the solid lines shows the full range (m_{start} to m_{end}) of evolutionary masses for the rotating solar metallicity models. The dashed lines mark the upper and lower mass ranges for the non-rotating solar metallicity models, while the dotted lines bracket the possible masses for the rotating LMC metallicity models and the dashed-dotted lines enclose the SMC metallicity models. Double encircled objects are located in the LMC.

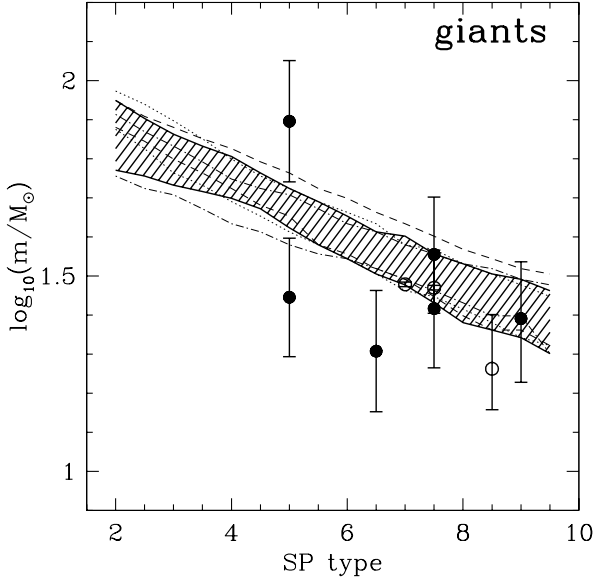


Fig. 5. Like Fig. 4 but for luminosity class III stars (giants).

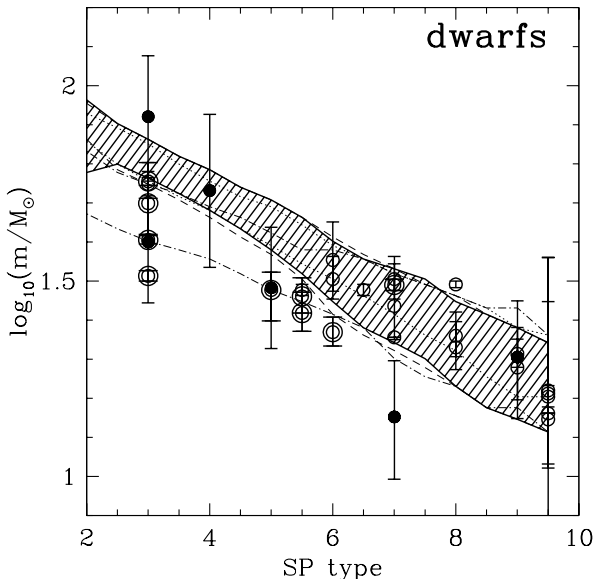


Fig. 6. Like Fig. 4 but for luminosity class V stars (dwarfs).

and maximal start and end ages for a given spectral class provide relevant information for statistical studies of roughly solar-metallicity young stellar populations. The relation derived here between spectral type and evolutionary mass agrees very well with dynamical as well as spectroscopic mass estimates for O stars from the literature and is therefore quite robust. No systematic discrepancy between dynamical, model and spectroscopic mass estimates could be found.

Because there are still considerable error margins in the new calibration, more observational and theoretical effort is necessary in order to improve on these. Larger samples of O stars with homogeneously derived parameters and larger sets of evolutionary models with a broader range of initial conditions (v_{rot} , metallicity, magnetic fields and, especially initial mass) would help to improve the calibration. Interestingly, seven out of nine stars located in the LMC (en-circled circles in Figs. 4 and 6) are below or at the lower end of the predicted evolutionary mass range. Even when considering an LMC metallicity luminosity- T_{eff} grid and evolutionary models (dashed lines in Figs. 4 to 6). These systematically lower dynamic masses could have several reasons. The influence of metallicity on the atmosphere and stellar models might be underestimated or these stars could be undetected contact systems instead of detached systems. Or stars earlier than O6 in the LMC are systematically misclassified and should all be shifted by one spectral subtype towards later types.

An additional startling fact are the low T_{eff} of the spectral type definitions for SMC metallicities and the resulting lower masses for early SMC O stars. This is probably because of the

lack of early O stars in the Heap et al. (2006) SMC study used here to calibrate the SMC spectral types. Yet these lower masses fit the eclipsing LMC (!) early O stars much better than the hot LMC spectral type definitions.

The other major source for uncertainties is massive binary evolution. It is a major obstacle, especially for giant and supergiant systems with dynamical mass estimates. These are generally short-period systems and the increasing radii of giants and supergiants during their evolution make mass transfer highly likely. Whilst the modelling of the relevant processes has significantly improved in recent years (Eldridge et al.

2008; Langer et al. 2008; de Mink et al. 2009; Song et al. 2009; van Rensbergen et al. 2010), the huge parameter space of hitherto unknown initial conditions (mass ratio, eccentricity, period, orbital inclination) and the possibility of reaching the same final state from different initial ones makes a correction for binary stellar evolutionary effects most challenging.

Given the internal consistency of the three model-dependent mass determinations (M_{evol} , M_{spec} and M_{wind}) it would be tempting to conclude that the basic properties of main-sequence O-type stars are now well understood. However, we point out that all that wind masses, the MSH05 calibrations, and the rotating Geneva stellar tracks all employ the same underlying mass-loss prescriptions of Vink et al. (2000), and these have recently been suggested to be too high (e.g. Fullerton et al. 2006) as a result of wind clumping. If calls for a fundamental downwards revision for O-star mass-loss rates were proven to be correct, this would undoubtedly result in the creation of new mass discrepancies. It may therefore be considered highly significant that current model masses seem to be backed up by model-independent dynamical masses – boosting confidence in our basic knowledge of the physical parameters, such as its mass-loss rate, and the modelling of the atmospheres and evolution of O-type stars.

Ironically it appears that the O-stars are currently better understood than the adjacent spectral type B-type stars, for which Cantiello et al. (2009, see their Fig. 10; with data from Trundle et al. (2007) and Hunter et al. (2008)) showed a highly significant mass discrepancy, with evolutionary masses up to a factor three larger than spectroscopic ones.

Acknowledgements. CW is happy to thank Jan Pfamm-Altenburg, Jim Dale, Nick Moeckel and Ian Bonnell for helpful discussions. This work made use of the Simbad web based database. This work was financially supported by the CONSTELLATION European Commission Marie Curie Research Training Network (MRTN-CT-2006-035890).

Appendix A: Stellar evolution

The evolution of stars used in this work is based on the stellar evolution models for solar and non-solar metallicity, rotating with 300 km/s and non-rotating by Meynet & Maeder (2003) and Meynet & Maeder (2005) and each two models with LMC and SMC metallicity (15 and 20 M_{\odot}) by Bertelli et al. (2009). Model tracks are only provided for stars with 9, 12, 15, 20, 25, 40, 60, 85 and 120 M_{\odot} for solar metallicity and even fewer for non-solar metallicity. As the lifetime of the stars and their respective evolutionary stages are dependent on the mass of the star, it is not possible to linearly interpolate between the track of a 40 and a 60 M_{\odot} star in order to get, for example, a 50 M_{\odot} star. Therefore, a special interpolation routine is employed here. The model tracks immediately above and below the target mass are normalized to their individual lifetimes (the point when the star becomes a neutron star or a black hole). Then the two normalized tracks are interpolated linearly to the target mass. The resulting track is then multiplied with the lifetime for the targeted star. This lifetime is linearly interpolated from the lifetime of the two input models.

Figure A.1 shows the stellar evolution of a 85 M_{\odot} and a 120 M_{\odot} star with time from Meynet & Maeder (2003) for several stellar parameters (luminosity, radius, mass, T_{eff}) together with an interpolated track of a 100 M_{\odot} star.

Appendix B: Spectral-type–stellar evolution tables

The following Table 9 shows the different spectral types that stellar evolution models reach during their lifetime. It uses so-

lar metallicity (Meynet & Maeder 2003) and non-solar metallicities (Meynet & Maeder 2005) and rotating ($v_{\text{rot,initial}} = 300$ km/s) and non-rotating tracks between 20 and 120 M_{\odot} . In this table are also shown evolutionary phases that go beyond the O spectral type used in the current work. Below we describe how these additional phases are classified. As the surface abundances for several species (H, He, C, N, O, Ne and Al) are also given in the models, it is possible to assign the beginning of the hydrogen-rich Wolf-Rayet phase (WNL) as soon the surface hydrogen abundance is below 60% (Hamann et al. 2006) and the helium-rich Wolf-Rayet phase (WNE) is given when the surface abundance of hydrogen is below 10^{-4} . Later on, stars are designated as carbon-rich Wolf-Rayet stars (WC) when helium starts to be depleted on the surface and the carbon abundance rises above 10^{-4} . Exceptions from this scheme are made when the stars enter the Luminous Blue Variable (LBV), Yellow Hyper-Giant (YHG), Yellow Giant (YG), Blue Supergiant (BSG) or Red Supergiant (RSG) phases. The hot end of the LBVs is defined by $\log_{10}(L_{\text{LBV hot}}) = 2.2056 \cdot \log_{10}(T_{\text{eff}}) - 3.7737$ and on the cool edge by $T_{\text{LBV cool}} = 7500$ K with a lower limit of $\log_{10}(L/L_{\odot}) = 5.3$ (Smith et al. 2004). YHGs lie between 4500 to 7500 K and $\log_{10}(L/L_{\odot}) \geq 5.3$ (Smith et al. 2004). Models that evolve between 4500 to 7500 K, but have $\log_{10}(L/L_{\odot}) < 5.3$, are named YGs. The BSGs are stars that are too cold for the O9.5 III or the O9.5 I types, but that are still below the LBV limit and hotter than YHGs. And finally, RSGs are stars colder than 4500 K and $\log_{10}(L) \geq 3.55 \log_{10}(L/L_{\odot})$ (Levesque 2010).

The evolutionary sequence for solar metallicity roughly agrees with the currently used observational sequence by e.g. Crowther (2007):

- $M_{\text{initial}} > 75 M_{\odot}$: O → WNL → LBV → WNE → WC → SNIC,
- $M_{\text{initial}} = 40 - 75 M_{\odot}$: O → LBV → WNE → WC → SNIC,
- $M_{\text{initial}} = 25 - 40 M_{\odot}$: O → LBV/RSG → WNE → SNIB.

Where SNIB and SNIC are supernovae type Ib and Ic, although it has recently been suggested that LBVs could explode early (Kotak & Vink 2006; Gal-Yam & Leonard 2009), which would significantly alter the later evolutionary phases of these types of schemes.

References

- Adams, F. C. & Myers, P. C. 2001, ApJ, 553, 744
 Allen, L., Megeath, S. T., Gutermuth, R., et al. 2007, in Protostars and Planets V, ed. B. Reipurth, D. Jewitt, & K. Keil, 361–376
 Apai, D., Bik, A., Kaper, L., Henning, T., & Zinnecker, H. 2007, ApJ, 655, 484
 Bertelli, G., Nasi, E., Girardi, L., & Marigo, P. 2009, A&A, 508, 355
 Bonanos, A. Z. 2009, ApJ, 691, 407
 Bouret, J., Lanz, T., & Hillier, D. J. 2005, A&A, 438, 301
 Burkholder, V., Massey, P., & Morrell, N. 1997, ApJ, 490, 328
 Cantiello, M., Langer, N., Brott, I., et al. 2009, A&A, 499, 279
 Castor, J. I., Abbott, D. C., & Klein, R. I. 1975, ApJ, 195, 157
 Conti, P. S. & Alsclher, W. R. 1971, ApJ, 170, 325
 Crowther, P. A. 2007, ARA&A, 45, 177
 de Mink, S. E., Cantiello, M., Langer, N., et al. 2009, A&A, 497, 243
 Eldridge, J. J., Izzard, R. G., & Tout, C. A. 2008, MNRAS, 384, 1109
 Evans, C. J. 2009, in IAU Symposium, Vol. 256, The Magellanic System: Stars, Gas, and Galaxies, ed. J. T. van Loon & J. M. Oliveira, 325–336
 Fernández Lajús, E. & Niemela, V. S. 2006, MNRAS, 367, 1709
 Fullerton, A. W., Massa, D. L., & Prinja, R. K. 2006, ApJ, 637, 1025
 Gabler, R., Gabler, A., Kudritzki, R. P., Puls, J., & Pauldrach, A. 1989, A&A, 226, 162
 Gal-Yam, A. & Leonard, D. C. 2009, Nature, 458, 865
 Gies, D. R. 2003, in IAU Symposium, Vol. 212, A Massive Star Odyssey: From Main Sequence to Supernova, ed. K. van der Hucht, A. Herrero, & C. Esteban, 91–+
- Groenewegen, M. A. T. & Lamers, H. J. G. L. M. 1989, A&AS, 79, 359

- Hamann, W.-R., Gräfener, G., & Liermann, A. 2006, A&A, 457, 1015
 Hanson, M. M., Howarth, I. D., & Conti, P. S. 1997, ApJ, 489, 698
 Heap, S. R., Lanz, T., & Hubeny, I. 2006, ApJ, 638, 409
 Herrero, A., Kudritzki, R. P., Vilchez, J. M., et al. 1992, A&A, 261, 209
 Hilditch, R. W., Harries, T. J., & Bell, S. A. 1996, A&A, 314, 165
 Hillier, D. J. 1991, A&A, 247, 455
 Hillier, D. J., Lanz, T., Heap, S. R., et al. 2003, ApJ, 588, 1039
 Hohle, M. M., Neuhäuser, R., & Schutz, B. F. 2010, Astronomische Nachrichten, 331, 349
 Hunter, I., Lennon, D. J., Dufton, P. L., et al. 2008, A&A, 479, 541
 Kobulnicky, H. A. & Fryer, C. L. 2007, ApJ, 670, 747
 Kotak, R. & Vink, J. S. 2006, A&A, 460, L5
 Kraus, S., Weigelt, G., Balega, Y. Y., et al. 2009, A&A, 497, 195
 Kudritzki, R., Hummer, D. G., Pauldrach, A. W. A., et al. 1992, A&A, 257, 655
 Lada, C. J. & Lada, E. A. 2003, ARA&A, 41, 57
 Lamers, H. J. G. L. M. & Leitherer, C. 1993, ApJ, 412, 771
 Langer, N., Cantiello, M., Yoon, S., et al. 2008, in IAU Symposium, Vol. 250, IAU Symposium, ed. F. Bresolin, P. A. Crowther, & J. Puls, 167–178
 Lanz, T., de Koter, A., Hubeny, I., & Heap, S. R. 1996, ApJ, 465, 359
 Levesque, E. M. 2010, in Astronomical Society of the Pacific Conference Series, Vol. 425, Hot and Cool: Bridging Gaps in Massive Star Evolution, ed. C. Leitherer, P. Bennett, P. Morris, & J. van Loon, 103–+
 Martins, F., Schaerer, D., & Hillier, D. J. 2005, A&A, 436, 1049
 Mayer, P., Drechsel, H., & Lorenz, R. 2005, ApJS, 161, 171
 Mayer, P., Harmanec, P., Nesslinger, S., et al. 2008, A&A, 481, 183
 Meynet, G. & Maeder, A. 2003, A&A, 404, 975
 Meynet, G. & Maeder, A. 2005, A&A, 429, 581
 Mokiem, M. R., de Koter, A., Evans, C. J., et al. 2007, A&A, 465, 1003
 Mokiem, M. R., de Koter, A., Evans, C. J., et al. 2006, A&A, 456, 1131
 Morrell, N. I., Barbá, R. H., Niemela, V. S., et al. 2001, MNRAS, 326, 85
 Niemela, V. S., Morrell, N. I., Fernández Lajús, E., et al. 2006, MNRAS, 367, 1450
 Preibisch, T., Balega, Y., Hofmann, K.-H., Weigelt, G., & Zinnecker, H. 1999, New Astronomy, 4, 531
 Puls, J., Kudritzki, R., Herrero, A., et al. 1996, A&A, 305, 171
 Repolust, T., Puls, J., & Herrero, A. 2004, A&A, 415, 349
 Ritchie, B. W., Clark, J. S., Negueruela, I., & Crowther, P. A. 2009, A&A, 507, 1585
 Sana, H., Momany, Y., Gieles, M., et al. 2010, A&A, 515, A26+
 Schweickhardt, J., Schmutz, W., Stahl, O., Szeifert, T., & Wolf, B. 1999, A&A, 347, 127
 Searle, S. C., Prinja, R. K., Massa, D., & Ryans, R. 2008, A&A, 481, 777
 Smith, N., Vink, J. S., & de Koter, A. 2004, ApJ, 615, 475
 Song, H. F., Zhong, Z., & Lu, Y. 2009, A&A, 504, 161
 Trundle, C., Dufton, P. L., Hunter, I., et al. 2007, A&A, 471, 625
 Vacca, W. D., Garmany, C. D., & Shull, J. M. 1996, ApJ, 460, 914
 van den Bergh, S. 2000, The Galaxies of the Local Group, ed. van den Bergh, S. (Cambridge)
 van Rensbergen, W., de Greve, J. P., Mennekens, N., Jansen, K., & de Loore, C. 2010, A&A, 510, 13
 Vink, J. S., de Koter, A., & Lamers, H. J. G. L. M. 2000, A&A, 362, 295
 Walborn, N. R., Howarth, I. D., Lennon, D. J., et al. 2002, AJ, 123, 2754
 Weidner, C., Kroupa, P., & Maschberger, T. 2009, MNRAS, 393, 663
 Williams, S. J., Gies, D. R., Henry, T. J., et al. 2008, ApJ, 682, 492
 Zorec, J., Cidale, L., Arias, M. L., et al. 2009, A&A, 501, 297

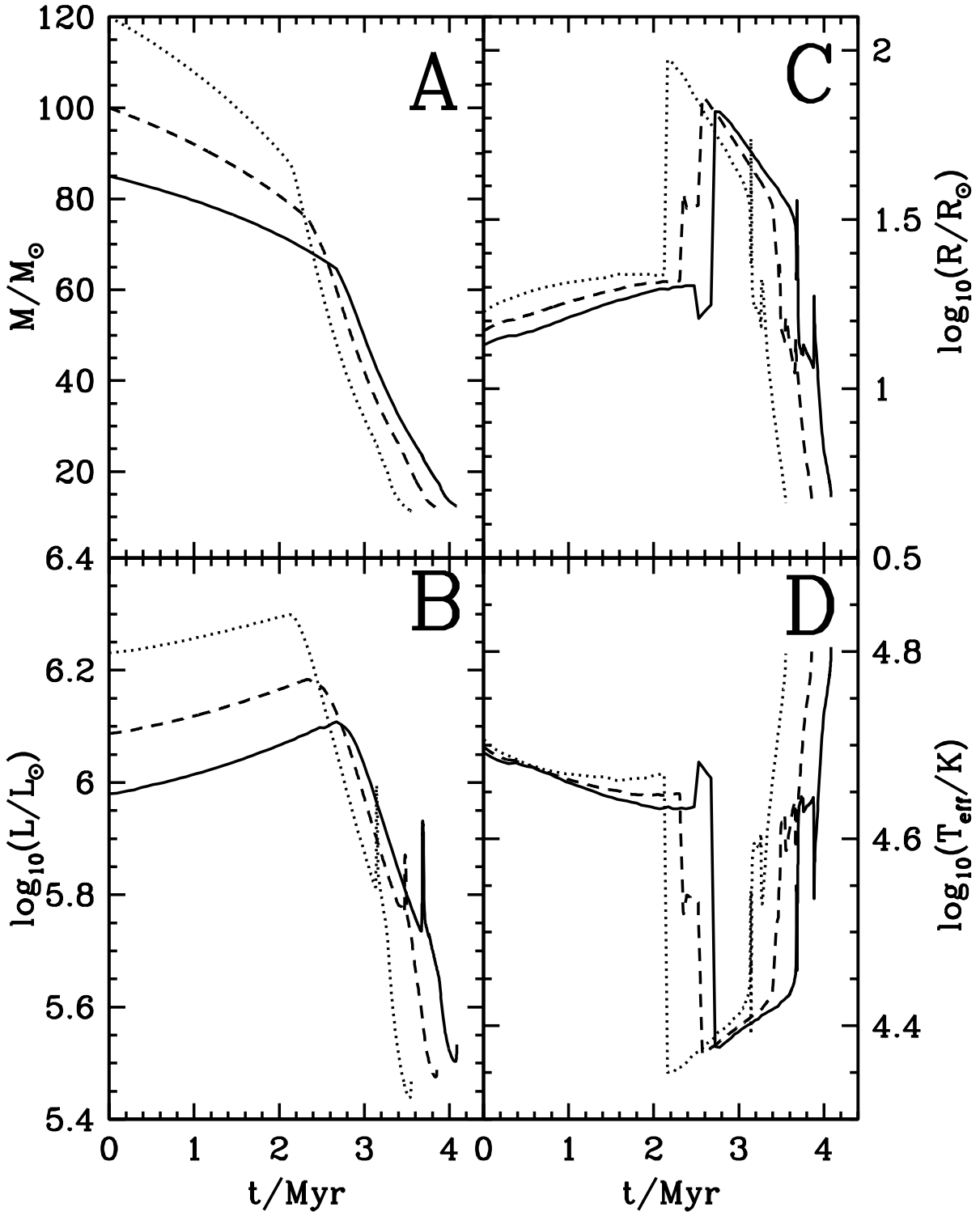


Fig. A.1. Panel A: Mass evolution over 4 Myr for a $85 M_{\odot}$ (solid line) and a $120 M_{\odot}$ star (dotted line) from literature data (Meynet & Maeder 2003). The dashed line shows a $100 M_{\odot}$ star interpolated from the two models. Panel B: Luminosity evolution over 4 Myr for the same three stars as in the panel A. Panel C: Radius evolution over 4 Myr for the same three stars as in panel A. Panel D: Effective temperature evolution over 4 Myr for the same three stars as in panel A.

Table 9. Spectral type evolution of stellar models.

Age Myr	mass M_{\odot}	Luminosity $\log_{10}(L/L_{\odot})$	T_{eff} $\log_{10}(\text{K})$	Sp. Type	Age Myr	mass M_{\odot}	Luminosity $\log_{10}(L/L_{\odot})$	T_{eff} $\log_{10}(\text{K})$	Sp. Type
solar metallicity ($z = 0.02$)									
$m_{\text{ini}} = 120 M_{\odot}, v_{\text{rot}} = 300 \text{ km/s}, z = 0.02$									
0.0000000	120.0000	6.2310	4.7050	O 2.0 If*	0.0000000	120.0000	6.2340	4.7120	O 2.0 If*
1.3778912	102.0845	6.2700	4.6660	WNL	1.1227475	107.0192	6.2530	4.6420	O 2.0 I
2.1617455	86.5949	6.2980	4.3500	LBV	1.2093965	105.8202	6.2550	4.6320	O 2.5 I
2.8960620	36.2371	5.9300	4.4030	WNL	1.2941639	104.6224	6.2580	4.6220	O 3.0 I
3.1424342	26.0184	5.9820	4.4230	LBV	1.4177116	102.8426	6.2620	4.6050	O 3.5 I
3.1458282	25.8019	5.9880	4.4350	WNL	1.4978035	101.6792	6.2650	4.5930	O 4.0 I
3.1906745	23.4728	5.8080	4.5920	WNE	1.6138339	99.9870	6.2700	4.5790	O 4.5 I
3.2641200	20.3641	5.7360	4.5750	WC	1.7257569	98.3582	6.2750	4.5630	O 5.0 I
3.5503435	11.2971	5.4710	4.7980	WC	1.7623851	97.8324	6.2770	4.5560	LBV
					2.7496870	41.2601	6.1690	4.5080	WNL
					2.7713165	38.9317	6.1310	4.5120	WNE
					2.7989238	36.2017	6.0930	4.5090	WC
					3.0980530	16.2928	5.7460	4.8130	WC
$m_{\text{ini}} = 85 M_{\odot}, v_{\text{rot}} = 300 \text{ km/s}, z = 0.02$									
0.0000000	85.0000	5.9800	4.6910	O 2.0 V	0.0000000	85.0000	5.9840	4.6990	O 2.0 If*
1.0302848	79.4176	6.0160	4.6590	O 2.0 III	0.1533940	84.3027	5.9870	4.6900	O 2.0 V
1.4552295	76.4990	6.0360	4.6450	O 2.5 I	0.9607395	80.0894	6.0100	4.6600	O 2.0 III
2.0694338	71.3398	6.0710	4.6320	WNL	1.2053038	78.6074	6.0190	4.6470	O 2.5 III
2.7229040	62.8013	6.1040	4.3780	LBV	1.2565218	78.2833	6.0200	4.6440	O 2.5 I
3.1913865	40.6504	5.9420	4.4060	WNL	1.4553924	76.9794	6.0280	4.6310	O 3.0 I
3.7471715	21.0334	5.7310	4.6420	WNE	1.5975672	76.0046	6.0340	4.6190	O 3.5 I
3.8772150	17.3227	5.6510	4.6420	WC	1.6891948	75.3598	6.0380	4.6090	O 4.0 I
4.0856488	12.3616	5.5330	4.8050	WC	1.8224420	74.4070	6.0440	4.5940	O 4.5 I
					1.9502418	73.4820	6.0510	4.5800	O 5.0 I
					2.0732452	72.5979	6.0570	4.5600	O 5.5 I
					2.1521198	72.0525	6.0620	4.5410	O 6.0 I
					2.2289090	71.5513	6.0670	4.5260	O 6.5 I
					2.3037808	71.0943	6.0730	4.5050	O 7.0 I
					2.4116148	70.5319	6.0810	4.4690	BSG
					2.4464302	70.3800	6.0840	4.4580	LBV
					3.1313858	39.1867	6.1750	4.5230	WNL
					3.1693195	36.0928	6.0530	4.5900	WNE
					3.1985408	33.6245	6.0170	4.5210	WC
					3.4635015	17.2654	5.7590	4.8010	WC
$m_{\text{ini}} = 60 M_{\odot}, v_{\text{rot}} = 300 \text{ km/s}, z = 0.02$									
0.0000000	60.0000	5.7020	4.6680	O 3.0 V	0.0000000	60.0000	5.7080	4.6750	O 3.0 V
0.1958980	59.6226	5.7080	4.6620	O 3.5 V	0.5715711	58.8823	5.7270	4.6590	O 3.5 V
1.3372419	56.9559	5.7600	4.6350	O 4.0 V	1.3906442	56.9734	5.7600	4.6350	O 4.0 V
1.6336100	56.0998	5.7760	4.6280	O 4.0 III	1.5717474	56.4936	5.7680	4.6280	O 4.0 III
2.4737502	53.1420	5.8290	4.6100	O 4.5 III	1.8594586	55.6850	5.7810	4.6140	O 4.5 III
2.7917235	51.7499	5.8530	4.6050	O 4.5 I	2.1249805	54.8898	5.7950	4.5980	O 5.0 III
2.9710480	50.8750	5.8660	4.6030	WNL	2.2265692	54.5749	5.8000	4.5900	O 5.0 I
3.9396822	44.1082	5.9510	4.3440	LBV	2.3720850	54.1169	5.8090	4.5770	O 5.5 I
4.2857995	32.3067	5.9200	4.3970	WNL	2.5574298	53.5309	5.8200	4.5570	O 6.0 I
4.3073855	31.2900	6.0210	4.4370	LBV	2.6887792	53.1230	5.8290	4.5400	O 6.5 I
4.3082900	31.2285	6.0620	4.4700	WNL	2.8151875	52.7477	5.8380	4.5200	O 7.0 I
4.3089005	31.1840	6.0690	4.4620	LBV	2.9347828	52.4192	5.8470	4.4980	O 7.5 I
4.3197685	30.3332	6.0900	4.4730	WNL	3.0123325	52.2268	5.8530	4.4800	O 8.0 I
4.3670145	27.5482	5.9130	4.6090	WNE	3.0857660	52.0650	5.8590	4.4610	O 8.5 I
4.4334785	24.1890	5.8570	4.5920	WC	3.1218755	51.9937	5.8620	4.4500	O 9.0 I
4.6809210	14.6686	5.6460	4.7990	WC	3.1912615	51.8739	5.8680	4.4280	O 9.5 I
					3.2612565	51.2141	5.8720	4.3950	BSG
					3.2947412	50.6178	5.8730	4.3720	LBV
					3.6153805	33.7033	5.8670	4.3750	BSG
					3.6224198	33.5101	5.8940	4.4460	O 9.0 I
					3.6229290	33.5080	5.9030	4.4550	O 8.5 I
					3.6233745	33.5060	5.9080	4.4530	O 9.0 I

Table 9. continued.

Age Myr	mass M_{\odot}	Luminosity $\log_{10}(L/L_{\odot})$	T_{eff} $\log_{10}(\text{K})$	Sp. Type	Age Myr	mass M_{\odot}	Luminosity $\log_{10}(L/L_{\odot})$	T_{eff} $\log_{10}(\text{K})$	Sp. Type
					3.6240875	33.5032	5.9100	4.4300	O 9.5 I
					3.6245332	33.4851	5.9090	4.3970	BSG
					3.6246225	33.4817	5.9100	4.3840	LBV
					3.6258830	33.1985	5.9280	3.8730	YHG
					3.6274002	32.9562	5.9930	3.9290	LBV
					3.6279472	32.7957	5.9760	3.8650	YHG
					3.6408085	28.8736	6.0340	3.8770	LBV
					3.6727700	26.6576	5.9840	4.4310	WNL
					3.7211365	24.5152	5.8540	4.6000	WNE
					3.8060685	21.0768	5.7380	4.6670	WC
					4.0147065	14.6174	5.6480	4.7950	WC
$m_{\text{ini}} = 40 M_{\odot}, v_{\text{rot}} = 300 \text{ km/s}, z = 0.02$					$m_{\text{ini}} = 40 M_{\odot}, v_{\text{rot}} = 0 \text{ km/s}, z = 0.02$				
0.0000000	40.0000	5.3410	4.6290	O 5.0 V	0.0000000	40.0000	5.3500	4.6380	O 5.0 V
0.6033284	39.6638	5.3650	4.6190	O 5.5 V	1.2306326	39.2770	5.3980	4.6160	O 5.5 V
2.7180158	37.9967	5.4770	4.5830	O 6.0 V	2.5606410	38.2461	5.4630	4.5830	O 6.0 V
2.8079328	37.9023	5.4830	4.5800	O 6.0 III	2.6943652	38.1257	5.4710	4.5780	O 6.0 III
3.5662060	37.0044	5.5360	4.5560	O 6.5 III	3.0685855	37.7742	5.4920	4.5600	O 6.5 III
3.9535328	36.4431	5.5660	4.5400	O 7.0 III	3.3507872	37.4991	5.5100	4.5430	O 7.0 III
4.1738048	36.0534	5.5850	4.5310	O 7.0 I	3.6131688	37.2431	5.5280	4.5220	O 7.5 III
4.4472590	35.5514	5.6090	4.5170	O 7.5 I	3.6630180	37.1954	5.5310	4.5170	O 7.5 I
4.7574220	34.9711	5.6390	4.4950	O 8.0 I	3.8064682	37.0616	5.5420	4.5020	O 8.0 I
4.9266050	34.6601	5.6570	4.4780	O 8.5 I	3.9426182	36.9415	5.5530	4.4850	O 8.5 I
5.0309235	34.4764	5.6690	4.4660	O 9.0 I	4.0279992	36.8714	5.5600	4.4720	O 9.0 I
5.1301465	34.3095	5.6800	4.4530	WNL	4.1534765	36.7774	5.5710	4.4530	O 9.5 I
5.5382560	32.8282	5.7780	4.3160	LBV	4.3112995	36.6785	5.5860	4.4220	BSG
5.5404720	32.5145	5.8030	3.8580	YHG	4.5648590	35.3579	5.6560	4.2690	LBV
5.6038870	23.6730	5.8910	4.2830	LBV	4.5651770	35.3557	5.6590	4.2420	BSG
5.6318410	22.4679	5.8770	4.3820	WNL	4.5681685	35.1705	5.6620	3.8600	YHG
5.7271790	19.2964	5.7050	4.6260	WNE	4.9779120	15.8704	5.6140	3.8970	LBV
5.7341225	19.0507	5.7060	4.6100	WC	4.9839990	15.4650	5.6120	4.5060	WNL
5.9676575	12.7371	5.5540	4.8000	WC	5.0102080	15.0283	5.6100	4.6520	WNE
					5.0534350	14.0897	5.6210	4.6460	WNE
$m_{\text{ini}} = 25 M_{\odot}, v_{\text{rot}} = 300 \text{ km/s}, z = 0.02$					$m_{\text{ini}} = 25 M_{\odot}, v_{\text{rot}} = 0 \text{ km/s}, z = 0.02$				
0.0000000	25.0000	4.8620	4.5660	O 7.0 V	0.0000000	25.0000	4.8730	4.5760	O 6.5 V
2.5403295	24.7687	4.9570	4.5460	O 7.5 V	0.7044491	24.9440	4.8940	4.5670	O 7.0 V
4.2112720	24.5183	5.0370	4.5270	O 8.0 V	3.1007708	24.7019	4.9880	4.5450	O 7.5 V
4.9560110	24.3579	5.0780	4.5130	O 8.5 V	4.1141835	24.5674	5.0360	4.5280	O 8.0 V
5.1965515	24.2999	5.0920	4.5080	O 8.5 III	4.7144740	24.4782	5.0670	4.5120	O 8.5 V
5.6416620	24.1845	5.1200	4.4950	O 9.0 III	4.9476720	24.4422	5.0810	4.5050	O 8.5 III
5.9484235	24.0992	5.1400	4.4840	O 9.5 III	5.1685970	24.4077	5.0940	4.4960	O 9.0 III
6.3443255	23.9827	5.1680	4.4660	BSG	5.4422980	24.3650	5.1110	4.4840	O 9.5 III
8.0793755	21.5113	5.3640	4.1330	LBV	5.6963615	24.3262	5.1270	4.4690	BSG
8.0813105	21.4602	5.3720	3.8720	YHG	6.6092615	24.1399	5.3040	4.0930	LBV
8.0819755	21.4540	5.3740	3.5900	RSG	6.6769850	23.4420	5.3060	3.8720	YHG
8.4990530	13.7862	5.5290	3.8550	YHG	6.7484280	22.9241	5.3000	3.6760	RSG
8.5055150	13.6556	5.5290	4.2870	WNL	7.2963415	16.6110	5.2570	3.5630	RSG
8.7131440	11.4163	5.4310	4.6900	WNE					
8.7183250	11.3330	5.4520	4.7010	WNE					
$m_{\text{ini}} = 20 M_{\odot}, v_{\text{rot}} = 300 \text{ km/s}, z = 0.02$					$m_{\text{ini}} = 20 M_{\odot}, v_{\text{rot}} = 0 \text{ km/s}, z = 0.02$				
0.0000000	20.0000	4.6100	4.5290	O 8.0 V	0.0000000	20.0000	4.6210	4.5400	O 7.5 V
1.2163962	19.9643	4.6410	4.5210	O 8.5 V	0.2819594	19.9930	4.6260	4.5360	O 8.0 V
4.0353365	19.8546	4.7370	4.5060	O 9.0 V	2.5817525	19.9281	4.6950	4.5210	O 8.5 V
5.8747015	19.7486	4.8150	4.4880	O 9.5 V	4.6272785	19.8518	4.7700	4.5040	O 9.0 V
6.7434725	19.6844	4.8580	4.4740	B 0.0 V	5.6688175	19.8048	4.8140	4.4890	O 9.5 V
7.2805585	19.6392	4.8870	4.4630	BSG	6.3578040	19.7711	4.8470	4.4740	B 0.0 V
10.1916910	18.0257	5.1440	3.8590	YG	6.8873955	19.7447	4.8740	4.4580	BSG
10.1918490	18.0252	5.1430	3.6040	RSG	8.4809040	18.8094	5.0720	3.8730	YG
11.0120840	11.7873	5.3870	3.5850	RSG	8.5819690	18.5271	5.0450	3.6020	RSG
					9.1767410	15.7450	5.0860	3.5600	RSG

Table 9. continued.

Age Myr	mass M_{\odot}	Luminosity $\log_{10}(L/L_{\odot})$	T_{eff} $\log_{10}(\text{K})$	Sp. Type	Age Myr	mass M_{\odot}	Luminosity $\log_{10}(L/L_{\odot})$	T_{eff} $\log_{10}(\text{K})$	Sp. Type
$z = 0.04$									
$m_{\text{ini}} = 120 M_{\odot}, v_{\text{rot}} = 300 \text{ km/s}, z = 0.04$									
0.0000000	120.0000	6.2810	4.7200	O 2If*	0.0000000	120.0000	6.2860	4.7270	O 2If*
0.7122990	106.1743	6.2800	4.7040	WNL	1.1811930	96.0022	6.2780	4.6690	WNL
1.5903378	83.8015	6.2800	4.3490	LBV	1.8489928	74.8679	6.2810	4.3330	LBV
2.0647445	41.2997	5.9280	4.4000	WNL	2.1893340	35.1802	5.9270	4.4010	WNL
3.0004895	12.6752	5.3520	4.6570	WNE	2.5832630	16.9112	5.5700	4.6230	WNE
3.2045120	9.8998	5.2310	4.6640	WC	2.7133730	13.5116	5.4550	4.6370	WC
3.4608532	7.1121	5.1160	4.8120	WC	3.0063900	8.5724	5.2650	4.8030	WC
$m_{\text{ini}} = 85 M_{\odot}, v_{\text{rot}} = 300 \text{ km/s}, z = 0.04$									
0.0000000	85.0000	6.0160	4.6700	O 2.0 V	0.0000000	60.0000	5.7630	4.6760	O 3.0 V
0.2073841	83.2480	6.0170	4.6610	O 2.0 III	1.6115779	52.5985	5.8280	4.6540	WNL
0.5546225	80.1208	6.0230	4.6450	O 2.5 III	3.9731632	11.5407	5.2770	4.6680	WNE
0.6112433	79.5865	6.0240	4.6430	O 2.5 I	4.2376410	8.7119	5.1460	4.6870	WC
0.9455716	76.2783	6.0320	4.6330	O 3.0 I	4.4505125	6.6861	5.0990	4.8100	WC
1.1074332	74.5755	6.0370	4.6310	WNL					
2.0882518	61.0788	6.0530	4.3290	LBV					
2.5212965	38.3726	5.8210	4.3630	WNL					
3.5020968	13.2380	5.3910	4.6520	WNE					
3.5656982	12.1506	5.3470	4.6570	WC					
3.9473910	7.2946	5.1400	4.8140	WC					
$m_{\text{ini}} = 60 M_{\odot}, v_{\text{rot}} = 0 \text{ km/s}, z = 0.04$									
0.0000000	60.0000	5.7490	4.6630	O 3.0 V	0.0000000	40.0000	5.3890	4.6190	O 5.0 V
0.2856618	59.0542	5.7550	4.6530	O 3.5 V	0.2346178	39.7772	5.3970	4.6160	O 5.5 V
0.7580356	57.3484	5.7690	4.6340	O 4.0 V	1.8258416	37.8880	5.4750	4.5820	O 6.0 V
0.8683556	56.9232	5.7730	4.6290	O 4.0 III	1.9091198	37.7668	5.4800	4.5800	O 6.0 III
1.1859810	55.6416	5.7840	4.6130	O 4.5 III	2.6890815	36.4932	5.5300	4.5560	O 6.5 III
1.4319508	54.5957	5.7940	4.5950	O 5.0 III	3.1912810	35.4259	5.5660	4.5400	O 7.0 III
1.5242232	54.1944	5.7980	4.5880	O 5.0 I	3.2596885	35.2664	5.5710	4.5370	WNL
1.6160245	53.7916	5.8020	4.5800	O 5.5 I	4.7375470	31.0692	5.7210	4.2620	LBV
1.8360944	52.8212	5.8130	4.5590	O 6.0 I	4.7952865	29.8853	5.8170	4.3600	WNL
1.9606289	52.2799	5.8200	4.5430	O 6.5 I	4.7958090	29.8715	5.8180	4.3480	LBV
2.0813522	51.7800	5.8270	4.5220	O 7.0 I	4.8024910	29.6620	5.9030	3.8750	YHG
2.2386800	51.1887	5.8380	4.4920	O 7.5 I	4.8570485	27.6540	5.9250	3.8760	LBV
2.3116478	50.9483	5.8440	4.4750	O 8.0 I	4.9483710	22.8732	5.8880	4.4330	WNL
2.3481315	50.8375	5.8470	4.4660	O 8.5 I	5.0142215	19.8232	5.7240	4.5940	WNE
2.3846155	50.7335	5.8500	4.4570	O 9.0 I	5.0210715	19.4902	5.7150	4.5960	WC
2.4523712	50.5647	5.8550	4.4330	O 9.5 I	5.3272680	11.4181	5.4850	4.8340	WC
2.5535530	49.2773	5.8580	4.3860	BSG					
2.5865480	48.4843	5.8570	4.3600	LBV					
3.0187062	33.1277	5.8510	4.3660	WNL					
3.1266585	29.0412	5.9810	4.4210	LBV					
3.1425120	27.8343	6.0130	4.4380	WNL					
3.1872218	24.6263	5.8430	4.5720	WNE					
3.2445090	21.0379	5.7580	4.5490	WC					
3.5380940	11.3294	5.4760	4.8120	WC					
$m_{\text{ini}} = 25 M_{\odot}, v_{\text{rot}} = 300 \text{ km/s}, z = 0.04$									
0.0000000	25.0000	4.9310	4.5710	O 6.5 V	0.0000000	25.0000	4.9410	4.5810	O 6.5 V
0.7839074	24.8724	4.9610	4.5650	O 7.0 V	1.8920445	24.6451	5.0200	4.5620	O 7.0 V
3.4727440	24.2181	5.1020	4.5410	O 7.5 V	3.2136872	24.3080	5.0880	4.5420	O 7.5 V
4.7023685	23.6354	5.1870	4.5230	O 8.0 III	3.9164080	24.0910	5.1300	4.5240	O 8.0 V
5.5065380	23.1187	5.2540	4.5060	O 8.5 III	4.1261118	24.0218	5.1430	4.5160	O 8.0 III
6.1294445	22.6320	5.3170	4.4890	O 9.0 III	4.2627490	23.9758	5.1520	4.5110	O 8.5 III
6.4360705	22.3614	5.3520	4.4790	WNL	4.5867530	23.8655	5.1750	4.4950	O 9.0 III
7.3809685	21.2317	5.5980	4.2400	LBV	4.8273150	23.7842	5.1930	4.4800	O 9.5 III
7.3820465	21.0639	5.6220	3.8730	YHG	5.0530525	23.7106	5.2100	4.4640	BSG
7.4232860	18.6763	5.7080	3.8770	LBV	5.8147580	23.5028	5.3230	4.4940	O 8.5 III
7.4467310	18.1922	5.7100	4.3290	WNL	5.8163300	23.5015	5.3150	4.4890	O 9.0 III
7.5964520	14.5465	5.5070	4.6330	WNE	5.8163300	23.5015	5.3150	4.4890	O 9.0 III
7.6086400	14.2369	5.4950	4.6350	WC	5.8170285	23.5010	5.3160	4.4750	O 9.5 III

Table 9. continued.

Age Myr	mass M_{\odot}	Luminosity $\log_{10}(L/L_{\odot})$	T_{eff} $\log_{10}(\text{K})$	Sp. Type	Age Myr	mass M_{\odot}	Luminosity $\log_{10}(L/L_{\odot})$	T_{eff} $\log_{10}(\text{K})$	Sp. Type
7.8694710	9.5879	5.3550	4.8140	WC	5.8178670	23.5004	5.3220	4.4520	BSG
					5.8241865	23.4506	5.3650	4.1410	LBV
					5.8282440	23.3195	5.3910	3.8720	YHG
					6.4117615	13.8709	5.4330	3.8500	YHG
$m_{\text{ini}} = 20 M_{\odot}, v_{\text{rot}} = 300 \text{ km/s}, z = 0.04$									
0.0000000	20.0000	4.6630	4.5210	O 8.5 V					
2.3022982	19.8656	4.7420	4.5060	O 9.0 V					
3.9294748	19.7344	4.8150	4.4890	O 9.5 V					
4.8387095	19.6420	4.8620	4.4740	B0.0 V					
5.3234640	19.5860	4.8890	4.4640	BSG					
8.1257930	17.7537	5.0520	4.3720	WNL					
8.6099200	16.8655	5.1760	3.9950	BSG					
8.6106560	16.8549	5.1750	3.8660	YG					
8.7348380	15.2882	5.3010	3.7260	YHG					
8.8588410	13.6160	5.3000	3.7630	YG					
9.1548770	9.8867	5.2440	4.4180	WNL					
9.4105940	9.2449	5.3520	4.4390	WNL					
LMC metallicity ($z = 0.008$)									
$m_{\text{ini}} = 120 M_{\odot}, v_{\text{rot}} = 300 \text{ km/s}, z = 0.008$									
0.0000000	120.0000	6.2140	4.7310	O 2.0 If*	0.0000000	60.0000	5.6820	4.6860	O 3.0 V
1.9595181	102.9785	6.3320	4.6760	WNL	0.2979827	59.6762	5.6950	4.6770	O 3.5 V
2.5262850	93.5009	6.3860	4.3640	LBV	0.7291670	59.1504	5.7170	4.6700	O 3.5 III
3.1879975	37.2673	6.0530	4.4570	WNL	2.0456922	56.9579	5.7980	4.6420	O 4.0 III
3.2485625	33.3330	6.0390	4.5960	WNE	2.3903512	56.1718	5.8240	4.6310	O 4.0 I
3.2724660	31.8841	6.0180	4.5790	WC	2.6550700	55.4854	5.8450	4.6210	O 4.5 I
3.2890230	30.4860	5.9900	4.4240	LBV	3.0891092	54.1722	5.8840	4.6000	O 5.0 I
3.2919092	30.0792	5.9740	4.4960	WC	3.4820080	52.7520	5.9230	4.5800	O 5.5 I
3.6300872	13.3927	5.5950	4.8180	WC	3.8287820	51.2107	5.9620	4.5620	WNL
					4.4030205	48.4254	6.0750	4.4590	LBV
					4.4045680	47.8923	6.1060	4.5100	WNL
					4.4048185	47.8903	6.1080	4.4800	LBV
					4.4081185	46.8239	6.1460	3.8770	BSG
					4.4090990	46.3901	6.1530	3.8750	YHG
					4.4110175	45.4902	6.1600	3.8770	LBV
					4.5355055	36.0793	6.1300	4.5000	WNL
					4.6174305	31.6506	6.0390	4.6050	WNE
					4.6207880	31.4079	6.0340	4.5980	WC
					4.6518545	29.8221	6.0070	4.2280	LBV
					4.6602595	26.1187	5.9310	4.4170	WC
					4.8432090	16.4456	5.7330	4.8490	WC
$m_{\text{ini}} = 40 M_{\odot}, v_{\text{rot}} = 300 \text{ km/s}, z = 0.008$									
0.0000000	40.0000	5.3170	4.6430	O 5.5 V	0.0000000	30.0000	5.0330	4.6080	O 6.5 V
2.3276098	39.0577	5.4390	4.6150	O 5.5 III	0.2138163	29.9785	5.0390	4.6050	O 7.0 V
3.1412225	38.5397	5.4930	4.5980	O 6.0 III	3.2977295	29.5309	5.1860	4.5780	O 7.5 V
3.7145050	38.0821	5.5360	4.5780	O 6.5 III	3.9570908	29.3825	5.2260	4.5670	O 7.5 III
4.0200750	37.8021	5.5610	4.5640	O 6.5 I	5.0176330	29.0838	5.2990	4.5380	O 8.0 III
4.0936185	37.7309	5.5680	4.5600	O 7.0 I	5.4466060	28.9076	5.3320	4.5190	O 8.5 III
4.4425960	37.3758	5.5990	4.5390	O 7.5 I	5.7691770	28.7612	5.3590	4.5010	O 9.0 I
4.6363970	37.1147	5.6180	4.5240	O 8.0 I	6.0574980	28.6264	5.3850	4.4800	O 9.5 I
4.8845875	36.7766	5.6430	4.5030	O 8.5 I	6.2608615	28.5321	5.4040	4.4620	BSG
5.0001165	36.6231	5.6550	4.4890	O 9.0 I	6.9819635	27.4565	5.5050	4.4630	O 9.5 I
5.1102935	36.4814	5.6670	4.4730	O 9.5 I	6.9829310	27.4558	5.5020	4.4610	BSG
5.2633395	36.2980	5.6850	4.4480	BSG	6.9879585	27.4354	5.5310	4.2160	LBV
5.6510235	35.2933	5.7580	4.4830	O 9.0 I	6.9905500	27.3408	5.5430	3.8650	YHG
5.6524505	35.2902	5.7560	4.4680	O 9.5 I	7.3154990	16.2920	5.6210	4.4620	WNL
5.6528645	35.2895	5.7580	4.4500	BSG	7.5867505	13.6902	5.5440	4.6940	WNE
5.6533780	35.2868	5.7650	4.4110	BSG	7.5963590	13.5216	5.5390	4.6890	WC
5.6541770	35.2744	5.7780	4.3290	LBV	7.6507400	12.1059	5.5420	4.6590	WC
5.6566830	35.0328	5.8000	3.8750	YHG					
5.7411655	28.4731	5.8650	3.8780	LBV					

Table 9. continued.

Age Myr	mass M_{\odot}	Luminosity $\log_{10}(L/L_{\odot})$	T_{eff} $\log_{10}(\text{K})$	Sp. Type	Age Myr	mass M_{\odot}	Luminosity $\log_{10}(L/L_{\odot})$	T_{eff} $\log_{10}(\text{K})$	Sp. Type
5.7845300	27.3243	5.8730	4.3750	WNL					
5.8047500	26.9017	5.8720	4.3660	LBV					
5.8336760	26.2948	5.8700	4.3730	WNL					
6.1551555	19.5713	5.7860	4.6640	WC					
6.2103525	17.3421	5.7650	4.7800	WC					
$m_{\text{ini}} = 20 M_{\odot}, v_{\text{rot.}} = 300 \text{ km/s}, z = 0.008, \text{Padova model}$									
0.0000000	19.6947	4.6294	4.5613	O 8.5 V					
1.5522020	19.6766	4.6652	4.5470	O 9.0 V					
5.3253110	19.6087	4.8051	4.5263	O 9.5 V					
7.2242600	19.5097	4.8985	4.4929	B					
7.5282720	19.4872	4.9155	4.4837	BG					
9.0765410	19.2730	5.0680	4.3931	BSG					
9.0885540	19.2641	5.0865	3.8735	YG					
9.0919190	19.2641	5.0451	3.6387	RSG					
9.1301450	19.2243	5.1754	3.6576	YG					
9.1327400	19.2243	5.1716	3.8853	BSG					
9.5183220	19.0173	5.1648	3.8710	YG					
9.5882510	18.9692	5.1509	3.6502	RSG					
9.7910080	18.7219	5.2919	3.5601	RSG					
SMC metallicity ($z = 0.004$)									
$m_{\text{ini}} = 120 M_{\odot}, v_{\text{rot.}} = 300 \text{ km/s}, z = 0.004$									
0.0000000	120.0000	6.2090	4.7450	O 2.0 If*	0.0000000	60.0000	5.6760	4.6980	O 2.0 If*
2.2878100	104.9922	6.3760	4.6680	WNL	1.6283401	58.4894	5.7700	4.6700	O 2.0 V
2.7973842	95.8416	6.4420	4.3910	LBV	2.2080835	57.6779	5.8110	4.6540	O 2.5 III
3.2331478	52.7831	6.3080	4.5710	WNL	2.6747342	56.8529	5.8490	4.6370	O 3.0 III
3.2714685	49.1669	6.2730	4.5860	WNE	2.9854308	56.1942	5.8760	4.6200	O 3.5 III
3.2810722	48.1992	6.2630	4.5220	LBV	3.1044190	55.9151	5.8880	4.6130	O 4.0 I
3.3344045	34.8949	6.0790	4.4690	WC	3.2770062	55.4829	5.9050	4.6010	O 4.5 I
3.5980968	17.1781	5.7530	4.7950	WC	3.4442515	55.0331	5.9220	4.5880	O 5.0 I
$m_{\text{ini}} = 40 M_{\odot}, v_{\text{rot.}} = 300 \text{ km/s}, z = 0.004$									
0.0000000	40.0000	5.3120	4.6550	O 3.5 V	3.5500428	54.7333	5.9340	4.5790	O 5.5 I
0.6528106	39.8576	5.3410	4.6460	O 4.0 V	3.7019615	54.2844	5.9510	4.5650	O 6.0 I
2.5598660	39.2560	5.4490	4.6270	O 4.5 V	3.8458675	53.8327	5.9680	4.5480	O 6.5 I
3.3546038	38.8721	5.5050	4.6090	O 5.0 V	3.9812960	53.3258	5.9840	4.5340	O 7.0 I
3.6820315	38.6794	5.5300	4.5990	O 5.0 III	4.1079905	52.8620	6.0000	4.5170	O 7.5 I
3.8373135	38.5797	5.5420	4.5930	O 5.5 III	4.1855345	52.5885	6.0110	4.5030	O 8.0 I
4.2053280	38.3209	5.5730	4.5760	O 6.0 III	4.2578970	52.3466	6.0200	4.4870	O 8.5 I
4.4137455	38.1603	5.5920	4.5630	O 6.5 III	4.3262125	52.1321	6.0300	4.4720	O 9.0 I
4.5455730	38.0540	5.6050	4.5540	O 6.5 I	4.3305155	52.1190	6.0310	4.4710	WNL
4.6090715	38.0016	5.6110	4.5490	O 7.0 I	4.4243485	51.8059	6.0720	4.4590	LBV
4.7954600	37.8387	5.6290	4.5320	O 7.5 I	4.4274385	51.2078	6.1040	3.8750	YHG
4.9154035	37.7017	5.6420	4.5210	O 8.0 I	4.4443775	44.5912	6.1620	4.2180	LBV
5.0891035	37.5044	5.6600	4.5020	O 8.5 I	4.6386520	35.9884	6.1270	4.5490	WNL
5.1982725	37.3843	5.6720	4.4870	O 9.0 I	4.6752050	34.2691	6.0890	4.2940	LBV
5.3033105	37.2729	5.6840	4.4700	O 9.5 I	4.6875580	34.2642	6.0950	4.5950	WNL
5.3987365	37.1772	5.6950	4.4530	BSG	4.7098275	33.9055	6.0960	4.4550	LBV
5.6899025	36.7542	5.7570	4.4720	O 9.0 I	4.7404865	32.5838	6.0880	4.6610	WNL
5.6909885	36.7519	5.7550	4.4670	O 9.5 I	4.7501970	32.0460	6.0800	4.6420	WNE
5.6918035	36.7506	5.7550	4.4480	BSG	4.7551630	31.7438	6.0760	4.6310	WC
5.6937425	36.7311	5.7740	4.3280	LBV	4.8120270	28.4654	6.0630	4.8410	WC
5.6965865	36.5473	5.7940	3.8750	YHG					
5.8482340	28.0283	5.8640	3.8760	LBV					
5.9362130	26.1314	5.8730	4.4130	WNL					
6.1748640	22.3331	5.8980	4.3890	WNL					
$m_{\text{ini}} = 20 M_{\odot}, v_{\text{rot.}} = 300 \text{ km/s}, z = 0.004, \text{Padova model}$									
0.0000000	19.6947	4.6301	4.5733	O 7.5 V	0.0000000	14.7724	4.2919	4.5249	O 9.5 V
0.6778070	19.6947	4.6479	4.5648	O 8.0 V	6.9185840	14.7622	4.4615	4.5012	B
5.5389360	19.6268	4.8283	4.5412	O 8.5 V	11.9532000	14.7214	4.6655	4.4266	BSG
6.5944990	19.5997	4.8804	4.5255	O 9.0 V	12.7442700	14.7045	4.7348	4.4348	B
7.3414660	19.5591	4.9215	4.5078	O 9.5 V	12.7579800	14.7045	4.7453	4.4276	BSG

Table 9. continued.

Age Myr	mass M_{\odot}	Luminosity $\log_{10}(L/L_{\odot})$	T_{eff} $\log_{10}(\text{K})$	Sp. Type	Age Myr	mass M_{\odot}	Luminosity $\log_{10}(L/L_{\odot})$	T_{eff} $\log_{10}(\text{K})$	Sp. Type
7.8724170	19.5276	4.9537	4.4893	B	12.7770200	14.7045	4.7461	3.8726	YG
8.2688160	19.5007	4.9807	4.4698	BG	12.7791200	14.7045	4.6056	3.6517	RSG
8.9886990	19.4111	5.0836	4.4244	BSG	12.9364100	14.6639	4.8698	3.6534	YG
9.6339610	19.1447	5.1912	3.8731	YG	12.9389100	14.6639	4.8960	3.8775	BSG
9.6607520	19.1227	5.1664	3.6523	RSG	13.7597900	14.5764	4.7932	3.8694	YG
					13.7622400	14.5764	4.6591	3.6501	RSG

Notes. Evolution of the Meynet & Maeder (2003) and Meynet & Maeder (2005) stellar models with and without rotation through the spectral types with a metallicity of $z = 0.02, 0.04, 0.008$ and 0.004 . The $20 M_{\odot}$ model with $z = 0.008$ and the 15 and $20 M_{\odot}$ models with $z = 0.004$ are from Bertelli et al. (2009).